

# *Driving factors of aerosol properties over the foothills of central Himalayas based on 8.5 years continuous measurements*

Article

Published Version

Hooda, R. K., Kivekäs, N., O'Connor, E. J., Collaud Coen, M., Pietikäinen, J.-P., Vakkari, V., Backman, J., Henriksson, S. V., Asmi, E., Komppula, M., Korhonen, H., Hyvärinen, A.-P. and Lihavainen, H. (2018) Driving factors of aerosol properties over the foothills of central Himalayas based on 8.5 years continuous measurements. *Journal of Geophysical Research: Atmospheres*, 123 (23). pp. 13421-13442. ISSN 2169-8996 doi: 10.1029/2018jd029744 Available at <https://centaur.reading.ac.uk/81444/>

It is advisable to refer to the publisher's version if you intend to cite from the work. See [Guidance on citing](#).

To link to this article DOI: <http://dx.doi.org/10.1029/2018jd029744>

Publisher: American Geophysical Union

All outputs in CentAUR are protected by Intellectual Property Rights law, including copyright law. Copyright and IPR is retained by the creators or other copyright holders. Terms and conditions for use of this material are defined in the [End User Agreement](#).

[www.reading.ac.uk/centaur](http://www.reading.ac.uk/centaur)

## **CentAUR**

Central Archive at the University of Reading

Reading's research outputs online

## RESEARCH ARTICLE

10.1029/2018JD029744

## Key Points:

- Long-term aerosol observations were conducted in the central Himalaya, and turbulence and water vapor were used to describe mixing layer diurnal cycle
- Aerosol variables clearly present clusters of highest concentration during the afternoon hours in the premonsoon and postmonsoon season
- Transport and valley wind influence to the atmospheric boundary layer are the predominant reasons for the poor performance of climate models

## Supporting Information:

- Supporting Information S1

## Correspondence to:

R. K. Hooda,  
rakesh.hooda@fmi.fi

## Citation:

Hooda, R. K., Kivekäs, N., O'Connor, E. J., Collaud Coen, M., Pietikäinen, J.-P., Vakkari, V., et al. (2018). Driving factors of aerosol properties over the foothills of central Himalayas based on 8.5 years continuous measurements. *Journal of Geophysical Research: Atmospheres*, 123, 13,421–13,442. <https://doi.org/10.1029/2018JD029744>

Received 3 OCT 2018

Accepted 9 NOV 2018

Accepted article online 14 NOV 2018

Published online 4 DEC 2018

## Author Contributions:

**Conceptualization:** R. K. Hooda

**Data curation:** R. K. Hooda

**Formal analysis:** R. K. Hooda, N. Kivekäs, M. Collaud Coen, V. Vakkari

**Funding acquisition:** R. K. Hooda, A.-P. Hyvärinen, H. Lihavainen

**Investigation:** R. K. Hooda

**Methodology:** R. K. Hooda, E. J. O'Connor, M. Collaud Coen, A.-P. Hyvärinen, H. Lihavainen

**Resources:** R. K. Hooda, E. J. O'Connor

**Supervision:** R. K. Hooda, N. Kivekäs, A.-P. Hyvärinen










**Validation:** R. K. Hooda, M. Collaud Coen, J.-P. Pietikäinen, J. Backman, S. V. Henriksson

**Visualization:** R. K. Hooda, N. Kivekäs

(continued)

©2018. American Geophysical Union.  
All Rights Reserved.

## Driving Factors of Aerosol Properties Over the Foothills of Central Himalayas Based on 8.5 Years Continuous Measurements

R. K. Hooda<sup>1,2</sup> , N. Kivekäs<sup>1</sup> , E. J. O'Connor<sup>1,3</sup> , M. Collaud Coen<sup>4</sup> , J.-P. Pietikäinen<sup>1</sup> , V. Vakkari<sup>1</sup> , J. Backman<sup>1</sup> , S. V. Henriksson<sup>1</sup> , E. Asmi<sup>1</sup>, M. Komppula<sup>5</sup>, H. Korhonen<sup>1</sup> , A.-P. Hyvärinen<sup>1</sup>, and H. Lihavainen<sup>1,6</sup>
<sup>1</sup>Finnish Meteorological Institute, Helsinki, Finland, <sup>2</sup>The Energy and Resources Institute, New Delhi, India, <sup>3</sup>University of Reading, Reading, UK, <sup>4</sup>Federal Office of Meteorology and Climatology, Payerne, Switzerland, <sup>5</sup>Finnish Meteorological Institute, Kuopio, Finland, <sup>6</sup>Now at SIOS-KC, Longyearbyen, Norway

**Abstract** This study presents analysis of in situ measurements conducted over the period 2005–2014 in the Indian Himalayas to give a thorough overview of the factors and causes that drive aerosol properties. Aerosol extensive properties (namely, particle number concentration, scattering coefficient, equivalent black carbon, PM<sub>2.5</sub>, and PM<sub>10</sub>) have 1.5–2 times higher values in the early to late afternoon than during the night, and a strong seasonality. The interannual variability is  $\pm 20\%$  for both PM<sub>2.5</sub> and total particle number concentration. Analysis of the data shows statistically significant decreasing trends of  $-2.3 \mu\text{g m}^{-3} \text{ year}^{-1}$  and  $-2.7 \mu\text{g m}^{-3} \text{ year}^{-1}$  for PM<sub>2.5</sub> and PM<sub>10</sub>, respectively, over the study period. The mountainous terrain site (Mukteshwar, MUK) is primarily under the influence of air from the plains. This is due to convective transport processes that are enhanced by local and mesoscale topography, leading to pronounced valley/mountain winds and consequently to atmospheric boundary layer air lifting from the plains below. The transport from plains is evident in seasonal-diurnal patterns observed at MUK. The timing of the patterns corresponds with changes in turbulence and water vapor ( $q$ ). According to our analysis, using these as proxies is a viable method for examining boundary layer influence in the absence of direct atmospheric boundary layer height measurements. Comparing the measurements with climate models shows that even regional climate models have problems capturing the orographic influence accurately at MUK, highlighting the importance of long-term direct measurements at multiple points to understand aerosol behavior in mountainous areas.

## 1. Introduction

Aerosols have been recognized as an important atmospheric constituent and an active climate forcing agent since the 1970s (Charlson et al., 1992; Twomey, 1977). Aerosols are highly nonuniform in the troposphere due to their relatively short residence times, variety of sources and sinks, and the chemical and microphysical processing that occurs in the atmosphere. Over the years, in spite of consistent improvements in instrumentation (both surface in situ and columnar measurements) and computational simulations, the single largest uncertainty continues to be aerosols in the estimation of globally averaged total radiative forcing (Intergovernmental Panel on Climate Change, 2007, 2013). The uncertainty further increases over regional scale by a factor about 2–4 across the regions—for example, black carbon (BC) estimations (Bond et al., 2013).

Almost 50% of the Earth's land surface is covered by hilly and mountainous terrain (Meybeck et al., 2001), and 27% is defined as mountainous (altitude  $> 1,500$  m above sea level, asl; Messerli & Ives, 1997). Thus, surface in situ observatory stations on mountains and in remote areas are important in addition to measurements in lowlands. High-altitude stations provide information on background aerosol properties in a larger area, trends in aerosol concentrations and properties, and data for validating models. Moreover, these stations are important in studying climatologies of aerosol radiative properties and the influence of regional sources and processes. However, over mountainous terrain, the atmospheric structure becomes much more complicated and even a universal definition of convective boundary layer (CBL) height over mountains remains an ambiguous issue (De Wekker & Kossmann, 2015; Rotach et al., 2015; Serafin et al., 2018). Transport and mixing processes, such as those related to mountain waves (Smith et al., 2007) and thermally driven wind systems (Zardi & Whiteman, 2013) among others, affect CBL variability significantly.

**Writing - original draft:** R. K. Hooda, A.-P. Hyvärinen

**Writing - review & editing:** R. K. Hooda, N. Kivekäs, M. Collaud Coen, V. Vakkari, E. Asmi, M. Komppula, H. Korhonen, A.-P. Hyvärinen, H. Lihavainen

The role of aerosols over the south Asian region (Di Girolamo et al., 2004; Lelieveld et al., 2001) has been a topic of high interest for the past two decades, and it is increasingly recognized as being among the hotspots of aerosols and anthropogenic trace gases; the anthropogenic emissions are relatively high in this region and expected to further increase for the next few decades (Dubash et al., 2018; IIASA, 2015; Krotkov et al., 2016; Ohara et al., 2007; Rao et al., 2016). In India, several focused and thematic campaigns such as Indian Middle Atmosphere Programme (Moorthy et al., 1999), Indian Ocean Experiment (Ramanathan et al., 2001), Indian Space Research Organization's Geosphere Biosphere Program (ISRO, 2004), and Integrated Campaign for Aerosols, gases and Radiation Budget (Satheesh et al., 2008) were conducted in the past. These campaigns addressed the physicochemical properties of aerosols and their modulation by mesoscale and synoptic meteorological processes at different geographical regions (Moorthy et al., 2016). Another recent campaign, Ganges Valley Aerosol Experiment, was carried out at Nainital to measure radiative, cloud, convection, and aerosol characteristics over the mainland for a 10-month period in 2011–2012 (Dumka et al., 2015; Kotamarthi, 2010; Singh et al., 2016). In spite of these efforts, the campaigns were time specific, and only a sufficiently long time series of data would help in inferring climate change signals (Moorthy et al., 2016). It is noticeable also that India is absent from the global map of GAW stations (WMO/GAW, 2016).

Notably, systematic and long-term measurements of aerosol properties in the Gangetic-Himalayan region in India were also performed by the Indo-Finnish cooperation of the Finnish Meteorological Institute and The Energy and Resources Institute at their sites: in the Himalayas at Mukteshwar (MUK) since 2005 (Collaud Coen et al., 2018; Henriksson et al., 2014; Hyvärinen et al., 2009; Komppula et al., 2009; Neitola et al., 2011; Nieminen et al., 2018; Panwar et al., 2013; Raatikainen et al., 2014; Raatikainen et al., 2017) and in the Indo Gangetic Plains (IGP) at Gual Pahari (GP) since 2007 (Baars et al., 2016; Hyvärinen et al., 2010; Hyvärinen, Raatikainen, Brus, et al., 2011; Hyvärinen, Raatikainen, Komppula, et al., 2011, 2013; Hooda et al., 2016; Komppula et al., 2012). These studies infer seasonality of aerosol properties based on surface in situ and columnar measurements, new particle formation events, topography characteristics, and disintegration between local and regional sources. The details can be obtained from each article since a critical review is not attempted in the present work; however, what is investigated as part of the present study has been highlighted as follows.

In this study, 8.5 years of measured aerosol physical and optical properties at a Himalayan site are analyzed. Remote sensing aerosol networks in India—for example, Aerosol Radiative Forcing over India Network and AERONET (Aerosol Robotic Network—are aerosol measurement programs started in early 2000, but to our knowledge, this data set at MUK represents the longest surface in situ aerosol observations from India which comprises physical and optical properties. We first provide an overview of the measurements, showing temporal variability of aerosol properties, which corroborate with the findings of distinct diurnal and seasonal cycles of our previous studies (refer above); however, those covered shorter time periods. We then focus on analyzing the possible factors and causes that drive aerosol diurnal, seasonal, and interannual variability and trends in aerosol properties at MUK. In particular, the long data set enables investigating the influence of valley/mountain winds and atmospheric boundary layer (ABL) dynamics on aerosol variability. For this purpose, a combination of micrometeorological observations of wind parameters, solar radiation, and water vapor is utilized. In addition, we used a global and a regional climate model to investigate how the changes in emission inventories over the study period relate to the observed long-term aerosol variability and to validate the climate model results against measurements at MUK.

## 2. Methods

### 2.1. Measurement Site

The measurement station, MUK (29°26'N, 79°37'E, 2,180 m asl) in India, is located in the foothills of the central Himalayas (Figure 1a). The site has a 180° view of the Himalayan ranges west, north, and east of the site; the nearest high peaks are approximately 90 km NE of the site. The area surrounding the site consists of low mountains (peaks 1,500–2,500 m asl) between the IGP (100–200 m asl) and the Himalayas (peaks 6,000–8,000 m asl; Figures 1b and S1 in the supporting information). The village of Mukteshwar, located 3 km NE of the measurement site and at a similar altitude, has ~800 inhabitants (Census of India, 2011). The nearest population centers are the town of Almora (1,650 m asl, 16 km N, population ~34,000) and Nainital (1,960 m asl, 25 km SW, population ~41,000) and the city of Haldwani (424 m asl, 32 km SW,

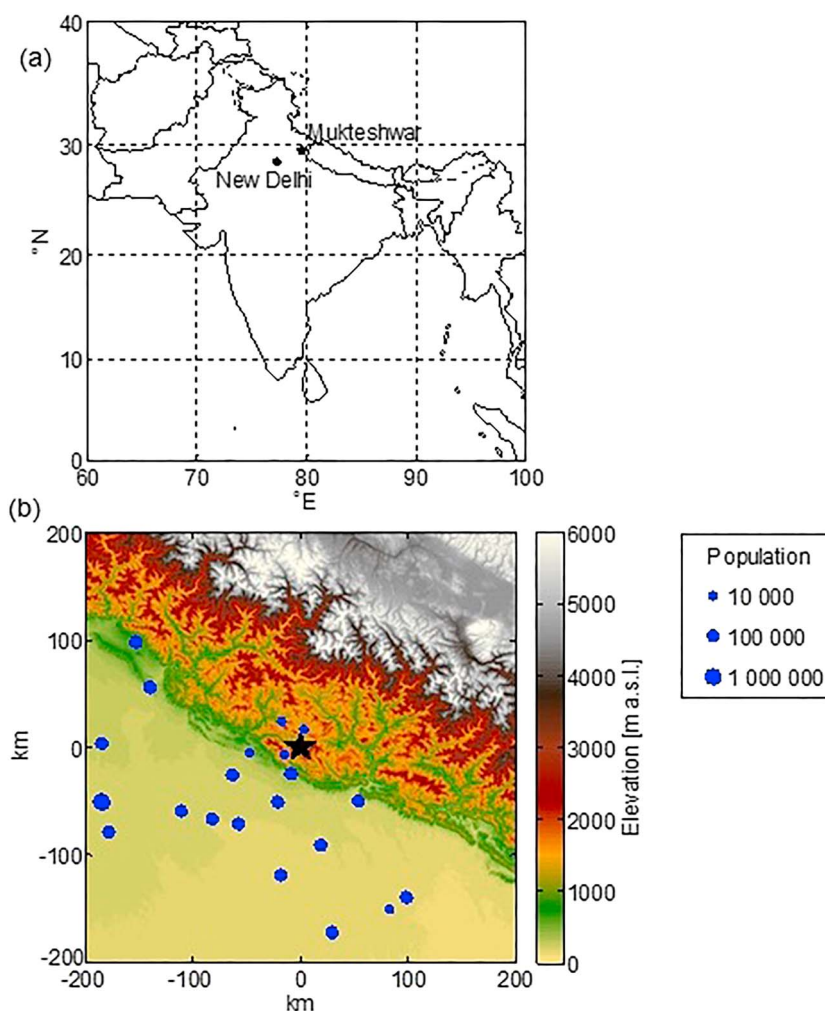


**Figure 1.** (a) Site location in India. (b) The location of Mukteshwar (denoted with star) and population centers (blue filled circles) on a 400 × 400 km topographic map (United States Geological Survey, 2016).

population ~150,000). The major metropolitan city Delhi (National Capital Territory), located in the IGP region (215 m asl, 250 km SW), has a population of ~16.8 million. Between Haldwani and Delhi, there are some industrial zones (Figure 1b), namely, the cities Kashipur and Rudrapur (70 km SW).

The IGP region is one of the most populated with over 900 million inhabitants. It is both highly fertile agricultural belt and a rapidly developing region of the Indian subcontinent. Furthermore, the geography of this region adds a considerable quantity of natural aerosols (windblown desert dust; Kumar, Kumar, et al., 2015, and reference therein) into the atmosphere from March to June, which coincides with anthropogenic ones, making the aerosol environment one of the most complex in the region (Moorthy et al., 2016). Crop residue burning over the IGP region is a common practice in clearing land during the harvesting period, resulting in highly seasonal agricultural particulate emissions (Kaskaoutis, Kumar, et al., 2014; Kumar et al., 2011; Rajput et al., 2014; Sahu et al., 2015; Singh & Kaskaoutis, 2014; Venkataraman et al., 2006). Considering the diverse fossil fuel use for domestic, industrial, and transport energy, and the open waste burning for disposal and heating purposes in this region (CPCB, 2010), especially over the IGP, the postmonsoon and winter seasons have also witnessed high pollution levels (Chakraborty et al., 2015; Hooda et al., 2016; Hyvärinen et al., 2010; Komppula et al., 2012). The elevated wintertime pollution levels as well as severe anthropogenic winter haze (Sati & Mohan, 2014) further coincide with the fog period (Ganguly et al., 2006; Gautam et al., 2007; Gautam & Singh, 2018), resulting in manifold increases in the complexity of aerosol composition over the region. These spatiotemporally diversified emissions are coupled with varying atmospheric dynamics, such as contrasting monsoons and varying ABL. All of this, together with the

complex topography, makes the Gangetic-Himalayan region's aerosol very difficult to fingerprint and model, and ultimately to implement effective mitigation strategies.

## 2.2. Aerosol Instrumentation and Data Processing

This study presents the aerosol time series from September 2005 to January 2014. The particle size distribution was measured using a differential mobility particle sizer (DMPS, Finnish Meteorological Institute assembled). A seven-wavelength (370 to 950 nm) Aethalometer (Magee Scientific AE-31) was used for measuring absorption coefficient ( $\sigma_{ap}$ ) and equivalent black carbon (eBC) at  $\lambda = 880$  nm, and an integrating nephelometer (Ecotech M 9003) measured the scattering coefficient ( $\sigma_{sp}$ ) at  $\lambda = 525$  nm. The particulate mass concentrations ( $PM_{2.5}$  and  $PM_{10}$ ) were measured with Thermo  $\beta$  attenuation mass monitors. The details of the instrumentation (supporting information Table S1) used in the present study, their maintenance and calibration protocols, and data logging are available in Hyvärinen et al. (2009) and Komppula et al. (2009). The ambient air sampling scheme and sample air conditioning (drying) adhered to the recommendations of World Meteorological Organization (WMO) (WMO/GAW, 2003, 2016) and have been detailed in our earlier publications (Hyvärinen et al., 2009; Komppula et al., 2009).

The DMPS data were divided into three characteristic particle size ranges of aerosol at MUK: 10- to 25-nm particles (nucleation-mode  $N_{nuc}$ ) represent the most recently formed aerosol particles, 25- to 90-nm particles (Aitken-mode  $N_{ait}$ ) represent fresher aerosol particles no more than a few days old, and 90- to 800-nm particles (accumulation-mode  $N_{acc}$ ) are representative of aged aerosol particles (Komppula et al., 2009; Seinfeld & Pandis, 2006). In general, particle number size distributions observed at MUK (Komppula et al., 2009) were mostly unimodal (with the mode at approximately 100 nm). The sum of the particle number concentrations in the three particle size ranges is termed  $N_{tot}$ . The particle mass concentration was also calculated utilizing the submicron aerosol size spectra assuming spherical particles and a gravimetric density of  $1.77 \text{ g/cm}^3$ . The density value used is representative for remote/background aerosols and is close to the bulk densities of ammonium sulphate and nitrate, the main constituents of accumulation-mode particles (DeCarlo et al., 2004; Heintzenberg et al., 2011; Stock et al., 2011). The mass size ranges are termed as  $M_{nuc}$ ,  $M_{ait}$ , and  $M_{acc}$  following the same diameter limits as in the number size distributions. The  $M_{acc}$  was calculated further for additional submicron particle mass concentration—for example, 90–200, 200–300, and 300–500 nm.

The truncation error inherent to the nephelometer was corrected using Mie scattering calculations following the guidelines of Anderson and Ogren (1998) and Moosmüller and Arnott (2003). The particle size range from 10 nm to the inlet cutoff diameter (i.e., 2.5 or 10  $\mu\text{m}$ ) was chosen for the correction using simultaneous (1.5 years) measured DMPS (mobility diameter) and Aerosol Particle Sizer, TSI 3321 (APS) (aerodynamic diameter) data. In May 2013, the common sample inlet was changed from  $PM_{2.5}$  to  $PM_{10}$ . The selection of the overlapped size channels in DMPS and APS is following Asmi et al. (2016). The correction factors (based on deemed inlet cutoff diameter) were estimated for the hourly data and averaged for those days and months when measurement coverage was  $\geq 50\%$ —that is, 12 hr/day and 15 days/month, respectively. The correction factors were then applied to different periods over the entire study time, in accordance with the deemed inlet cutoff diameter installed for nephelometer measurements. The truncation error of the measured  $\sigma_{sp}$  varies between 11% and 12% across the seasons, and an error of up to 5%–15% is acceptable depending on the particle size (Anderson et al., 1996).

The aethalometer measurements are known to suffer from several artifacts (namely, multiple scattering enhancement on the filter tape corrected by using a C factor and loading effect referred to as the shadowing effect). The approach of Weingartner et al. (2003) for these artifact corrections was applied in the present analysis following Hyvärinen et al. (2009), utilizing a C factor of 2.14. However, Collaud Coen et al. (2010) and in year 2016, WMO/Global Atmosphere Watch (GAW) has evaluated new aethalometer correction schemes and concluded that the C factor used in most studies worldwide is too low and should be at least 2.9 (Collaud Coen et al., 2010) or 3.5 (WMO/GAW, 2016). The latter value is generally likely to be adopted, in principle, and has an uncertainty of approximately 25% (Müller, 2015; WMO/GAW, 2016). To keep our data set consistent with the previous analysis (Hyvärinen et al., 2009), we report our results with a C factor of 2.14 (Weingartner et al., 2003). However, the results with a C factor of 3.5 show repercussions on aerosol intensive properties (such as the single scattering albedo); thus, we have discussed these as well.



The single scattering albedo (SSA) using measured  $\sigma_{sp}$  ( $\lambda = 525$  nm) and  $\sigma_{ap}$  ( $\lambda = 520$  nm), and absorption Ångström exponent ( $\alpha_{abs}$ ) that describes the spectral dependence of light absorption by the aerosol (Müller et al., 2011) was calculated. The  $\alpha_{abs}$  is the negative slope of the regression fit between the logarithm of the absorption coefficients and the logarithm of the wavelengths (seven wavelengths between 370 and 950 nm).

The annual coverage of valid and analyzable hourly averaged data (processed/screened) of different aerosol properties and meteorological parameters is presented in supporting information Table S1. During data processing, the meteorological and aerosol parameters were averaged to 1-hr resolution, taking into account only those hours when more than 50% of the time was covered by valid measurements.

To extract more information on the seasonally averaged diurnal cycles, the diurnal cycles of the aerosol parameters were separated from the monthly background values and are denoted as  $e\Delta$  and  $i\Delta$  for extensive and intensive, respectively. This was done by subtracting mean monthly minima of the diurnal values from each monthly diurnal cycle. This procedure forces the minimum value of the  $e\Delta$  to be zero for the diurnal cycles of each month. These minimum values were systematically observed early in the morning before sunrise. As the minimum values of aerosol intensive parameters were typically observed at different times of the day for different months and for different parameters,  $i\Delta$  was calculated by subtracting the mean monthly 5:00 a.m. value (representing the time before the onset of the increase in particle concentration) from each monthly cycle.

### 2.3. Meteorological Data and Mixing Layer

The measurements of meteorological parameters (i.e., temperature, pressure, relative humidity, wind speed, wind direction, and global solar irradiance) were done using MILOS500+ sensors (Vaisala). Daily precipitation data was collected from the India Meteorological Department weather station, less than 2 km NE of MUK. The seasonal classification adopted for MUK is winter (December to February), premonsoon (March to May), monsoon (July to August), postmonsoon (October to November), and the transition months between monsoon and other seasons (June and September). The solar zenith and azimuth angles were also calculated using the algorithm of Blanco-Muriel et al. (2001) for representation of sunrise and sunset time in aerosol variability cycles.

The specific humidity can be used as a passive tracer (Kowol-Santen et al., 2001; Serafin et al., 2018; Weigel et al., 2007) to examine the ABL dynamics. It was calculated using meteorological data as shown in equation (1), following Bolton, (1980), and used in the present study when direct measurements of mixing layer depth (height) at MUK are not available.

$$q = \frac{(0.622 \times e)}{(p - (0.378 \times e))}; e = 6.112 \times \exp\left(\frac{(17.67 \times Td)}{(Td + 243.5)}\right), \quad (1)$$

where  $q$  is the specific humidity in kg/kg,  $p$  is the surface pressure in hectopascals,  $e$  is the vapor pressure in hectopascals,  $Td$  = dew point in °C, and the final specific humidity units are in g/kg.

Together with  $q$  (referred to as water vapor in from here onwards), wind speed and direction and solar radiation were also used for investigating ABL dynamics at MUK. For part of the same period, water vapor was also measured at GP (28°26'N, 77°09'E, 243 m asl), located in the IGP region near Delhi at 270-km distance from MUK (Hooda et al., 2016). In wind parameters, we utilized wind direction variability ( $\delta_{WD}$ ) and relative wind speed variability ( $\delta_{WSr}$ ). The  $\delta_{WD}$  was calculated as the average of the absolute differences in wind direction from 1 min to the next during the given hour. The  $\delta_{WSr}$  was calculated similarly to  $\delta_{WD}$ , but in the end, it was divided by the average wind speed that hour in order to retrieve a proxy that was independent of the mean wind speed. In the case of the water vapor ( $q$ ), its variability was obtained by subtracting the monthly mean diurnal minima from the monthly mean diurnal cycle and denoted as  $\partial q$ . Further, to investigate the ABL air lifting from the plains below, we also examined  $\partial q$  at GP and utilized average diurnal cycle of water vapor at GP for each month for further analysis. The variability (denoted as  $\partial q$ ) in water vapor at MUK and GP shows some unique differences (see Figures 5f and S2d, respectively). We assumed that  $\partial q$  at the GP site represents the typical water vapor values in the plains (IGP). Each hourly water vapor value at MUK was then subtracted from the corresponding hourly water vapor value at GP. This difference was noted as

$\phi q$ . We assumed, as stated earlier, that early in the morning (5:00 a.m.), there is no mixing of air between the plains and MUK and noted the  $\phi q$  at 5:00 a.m. as  $\Delta MPq$ , the undisturbed difference of  $q$  between MUK and the plains. The fraction of MUK air originating from the plains ( $\Phi q$ ), a clear indicator, was then calculated according to equation (2):

$$\left[ \Phi q = 1 - \frac{(q_{GP} - q_{MUK})}{(\Delta MPq)} \right]; \quad (2)$$

#### 2.4. Back Trajectories and Modeled Mixing Layer Depth

Lagrangian models are often used to investigate source-receptor relationships based on air mass movement from gridded meteorological data (Fleming et al., 2012). In order to investigate the origin of the air masses measured at MUK, 5-day back trajectories were calculated using the Hybrid Single-Particle Lagrangian Integrated Trajectory model version 4.9 (Draxler & Hess, 1998; Stein et al., 2015). The meteorological data used was the 1° National Center for Environmental Prediction (NCEP)/Global Data Assimilation System (GDAS) data set with 23 hybrid pressure levels (Kanamitsu, 1989). The 5-day back trajectories were calculated for every 3 hr (the temporal resolution of the GDAS data) over the years 2005–2014. The mixing layer depth was taken from the NCEP/GDAS and this is referred to as modeled mixing layer depth from here onwards.

#### 2.5. Statistical Analysis

The statistical methods were used to analyze the trends of aerosol parameters at MUK and to verify the sensitivity of the trends results. Since the aerosol variables are approximately lognormally distributed, a nonparametric trend test and slope estimator, the seasonal Mann-Kendall (MK) test and the Sen's slope estimator (Collaud Coen et al., 2013), were applied to the daily data to detect potential long-term trends and their magnitudes for each month as well as for the whole data sets. The least mean squares (LMS) fit of the logarithm of the monthly median has been widely used for trends estimations (Collaud Coen et al., 2007; Collaud Coen et al., 2013), and this was also applied in the present analysis. With these statistical tools, a general picture of the aerosol long-term variability can be obtained. If a trend was detected by one of the methods, a generalized least squares (GLS) trend with either autoregressive or block bootstrap (ARB) confidence intervals (Asmi et al., 2013) was also applied to validate the trend and estimate its magnitude. The trend analysis was also performed with the same methods on the meteorological parameters as they were recorded, since these are usually normally distributed. The trend analysis performed on aerosol and meteorological parameters was for the period September 2005 to January 2014 (about 8.5 years), except for DMPS, aethalometer and nephelometer. In May 2013, the common sample inlet of these instruments was changed from PM<sub>2.5</sub> to PM<sub>10</sub> leading to a break in the long-term data set of absorption and scattering coefficients. Thus, for these parameters, the trend analysis was applied to the period of September 2005 to May 2013 (about 7.8 years). The DMPS data could only be considered homogeneous from March 2006 to November 2012, and therefore, the trend analysis was applied to this shorter data set of about 6.8 years.

#### 2.6. Global and Regional Model Simulations

The global aerosol-climate model ECHAM-HAMMOZ (version ECHAM6.1.0-HAM2.2.0-MOZ0.9.0) was used with interactive aerosols to simulate years 2004–2014 with T63 (~210 km/1.9° grid box) spatial resolution and 31 vertical levels (Zhang et al., 2012). ECHAM-HAMMOZ accounts for both direct and indirect aerosol effects. The model simulations were nudged (vorticity, divergence, temperature, and surface pressure) towards ERA-Interim data (Dee et al., 2011). For anthropogenic emissions, ECLIPSE (Evaluating the Climate and Air Quality Impacts of Short-Lived Pollutants (ECLIPSE)) emission data (IIASA, 2015) was used. Detailed treatment of the emissions in ECHAM-HAMMOZ, including the annual cycle imposed on the domestic sector emissions, can be found in Pietikäinen et al. (2015). The wildfire emissions were taken from Global Fire Emissions Database v4 (van der Werf et al., 2010) as monthly average fields. Other natural emissions were taken as shown in Stier et al. (2005) and Zhang et al. (2012). Natural as well as aircraft emissions were used, as in Matt et al. (2016).

The regional aerosol-climate model REMO-HAM (version REMO2009; Pietikäinen et al., 2012) with interactive aerosols was simulated for 2007–2011 including a spin-up time, using 0.22° (~25 km grid box) resolution with 27 vertical levels covering plains and the Himalayas in India. More details about the domain can be seen in Kumar, Kotlarski, et al. (2015). Currently, aerosols in REMO-HAM impact radiation only through clouds



**Table 1**  
Seasonal/Annual Values (Mean  $\pm$  SD) of Aerosol Extensive and Intensive Parameters at MUK

Aerosol property	Winter (DJF)	Premonsoon (MAM)	Monsoon (Jul–Aug)	Postmonsoon (ON)	Transition (Jun and Sep)	Annual
<b>Extensive</b>						
PM <sub>2.5</sub> ( $\mu\text{g}/\text{m}^3$ )	20 $\pm$ 10	40 $\pm$ 20	12 $\pm$ 10	22 $\pm$ 15	25 $\pm$ 15	25 $\pm$ 15
PM <sub>10</sub> ( $\mu\text{g}/\text{m}^3$ )	25 $\pm$ 20	70 $\pm$ 40	20 $\pm$ 25	35 $\pm$ 25	40 $\pm$ 30	40 $\pm$ 30
eBC ( $\mu\text{g}/\text{m}^3$ )	0.85 $\pm$ 0.65	1.40 $\pm$ 0.85	0.35 $\pm$ 0.25	0.90 $\pm$ 0.60	0.70 $\pm$ 0.40	0.90 $\pm$ 0.60
<sup>a</sup> $\sigma_{\text{ap}}$ ( $\text{Mm}^{-1}$ ) <sup>2.14</sup>	12 $\pm$ 9	20 $\pm$ 10	5 $\pm$ 3	12 $\pm$ 8	10 $\pm$ 6	12 $\pm$ 8
<sup>a</sup> $\sigma_{\text{ap}}$ ( $\text{Mm}^{-1}$ ) <sup>3.5</sup>	7 $\pm$ 6	12 $\pm$ 7	3 $\pm$ 2	7 $\pm$ 5	6 $\pm$ 3	7 $\pm$ 5
$\sigma_{\text{sp}}$ ( $\text{Mm}^{-1}$ )	70 $\pm$ 60	110 $\pm$ 65	35 $\pm$ 30	75 $\pm$ 60	65 $\pm$ 40	75 $\pm$ 55
$N_{\text{tot}}$ ( $\text{cm}^{-3}$ )	2,700 $\pm$ 1,700	5,200 $\pm$ 2,850	1,650 $\pm$ 750	2,200 $\pm$ 1,100	2,600 $\pm$ 1,250	3,050 $\pm$ 1,650
$N_{\text{nuc}}$ ( $\text{cm}^{-3}$ )	90 $\pm$ 120	380 $\pm$ 600	40 $\pm$ 45	65 $\pm$ 85	80 $\pm$ 125	150 $\pm$ 200
$N_{\text{ait}}$ ( $\text{cm}^{-3}$ )	1,200 $\pm$ 820	2,290 $\pm$ 1520	840 $\pm$ 360	880 $\pm$ 550	1,240 $\pm$ 670	1,360 $\pm$ 850
$N_{\text{acc}}$ ( $\text{cm}^{-3}$ )	1,420 $\pm$ 950	2,550 $\pm$ 1450	770 $\pm$ 420	1,200 $\pm$ 600	1,320 $\pm$ 680	1,540 $\pm$ 880
<b>Intensive</b>						
$\alpha_{\text{abs}}$	1.40 $\pm$ 0.5	1.25 $\pm$ 0.2	1.15 $\pm$ 0.3	1.20 $\pm$ 0.3	1.10 $\pm$ 0.3	1.25 $\pm$ 0.4
<sup>b</sup> SSA <sup>2.14</sup>	0.82 $\pm$ 0.06	0.84 $\pm$ 0.03	0.83 $\pm$ 0.07	0.83 $\pm$ 0.04	0.84 $\pm$ 0.06	0.83 $\pm$ 0.05
<sup>b</sup> SSA <sup>3.5</sup>	0.88 $\pm$ 0.05	0.90 $\pm$ 0.02	0.89 $\pm$ 0.06	0.89 $\pm$ 0.03	0.90 $\pm$ 0.05	0.89 $\pm$ 0.04
PM <sub>2.5</sub> /PM <sub>10</sub>	0.97 $\pm$ 0.63	0.68 $\pm$ 0.31	0.88 $\pm$ 0.73	0.94 $\pm$ 0.58	0.79 $\pm$ 0.55	0.85 $\pm$ 0.55
eBC/PM <sub>2.5</sub>	0.06 $\pm$ 0.07	0.04 $\pm$ 0.03	0.07 $\pm$ 0.06	0.05 $\pm$ 0.07	0.04 $\pm$ 0.04	0.05 $\pm$ 0.05
$N_{\text{acc}}/N_{\text{tot}}$	0.5 $\pm$ 0.1	0.5 $\pm$ 0.1	0.4 $\pm$ 0.1	0.6 $\pm$ 0.1	0.5 $\pm$ 0.1	0.5 $\pm$ 0.1
$N_{\text{ait}}/N_{\text{acc}}$	1.3 $\pm$ 0.6	1.4 $\pm$ 0.8	1.8 $\pm$ 1.0	1.1 $\pm$ 0.6	1.4 $\pm$ 0.8	1.05 $\pm$ 0.6

Note. The 2.14 value of  $C$  (Weingartner et al., 2003) and 3.5 value of  $C$  (WMO/GAW, 2016) used in Weingartner correction (Weingartner et al., 2003) approach for the aethalometer. DJF = December to February; MAM = March to May; ON = October to November; SSA = single scattering albedo; eBC = equivalent black carbon. <sup>a</sup>For hourly data, the value of  $\sigma_{\text{ap}}$  is decreased by 40% on average (range 25% to 45%). <sup>b</sup>Single scattering albedo (SSA) is increased by 7% (range 3% to 10%) while using  $C = 3.5$  instead of using  $C = 2.14$  (see section 2.2 on  $C$  factor correction).

(indirect effects). The ERA-Interim data were used as lateral boundary for meteorology, and the data from ECHAM-HAMMOZ simulations (as above) were postprocessed for REMO's aerosol boundary forcing data. The same ECLIPSE aerosol emissions as discussed above were used in REMO-HAM. The shorter period of simulations in REMO-HAM versus ECHAM-HAMMOZ is due to the heavier computational burden as a result of higher resolution.

### 3. Results and Discussion

#### 3.1. Aerosol Variability

We summarize first the characteristics of the observed aerosol variability over 8.5 years of continuous measurements. Distinct diurnal and seasonal cycles are observed for the extensive (particle number concentration, scattering coefficient, eBC, PM<sub>2.5</sub>, and PM<sub>10</sub>) and the intensive ( $\alpha_{\text{abs}}$ , SSA, and geometric mean diameter [GMD]) aerosol parameters. The seasonal and diurnal variations exhibit many similarities during 8.5 years of measurements. The drivers of these variabilities are discussed in section 3.2.

##### 3.1.1. Seasonal-Diurnal Cycle

Both extensive and intensive aerosol parameters manifest a pronounced month-dependent diurnal cycle. Table 1 displays a strong seasonality across the aerosol properties similar to that presented earlier (Hyvärinen et al., 2009; Komppula et al., 2009; Raatikainen et al., 2014) for optical and physical properties based on a data set of 2–3 years at MUK. Recently, Dumka et al. (2015) also perceived a similar seasonality in scattering and absorption coefficients at Nainital based on 10-month observations.

In premonsoon months, the concentration of extensive aerosol properties is consistently high over the course of the day with 1.5–2 times higher values in the early to late afternoon than during the night (Figure 2, left column). However,  $N_{\text{nuc}}$  is exceptional for different reasons (discussed later). The consistently higher values of aerosol, as seen in the left panel of Figure 2, exhibit attribution of high background/residual aerosol concentration in premonsoon, which may be misinterpreted as a weakened diurnal pattern. Notably in normalized analysis ( $\epsilon\Delta$  and  $\Delta$  values; Figure 2, right column), the influence of long-range transported aerosols in the late afternoon dominates distinctly during premonsoon, when air masses from the plains reach MUK (see section 3.2). This is evidenced by relatively large amplitudes in  $N_{\text{tot}}$ , PM<sub>2.5</sub>, eBC, and  $\sigma_{\text{sp}}$  values in corresponding time (Figure 2, right column). In the case of  $N_{\text{nuc}}$  (Figure 2c)

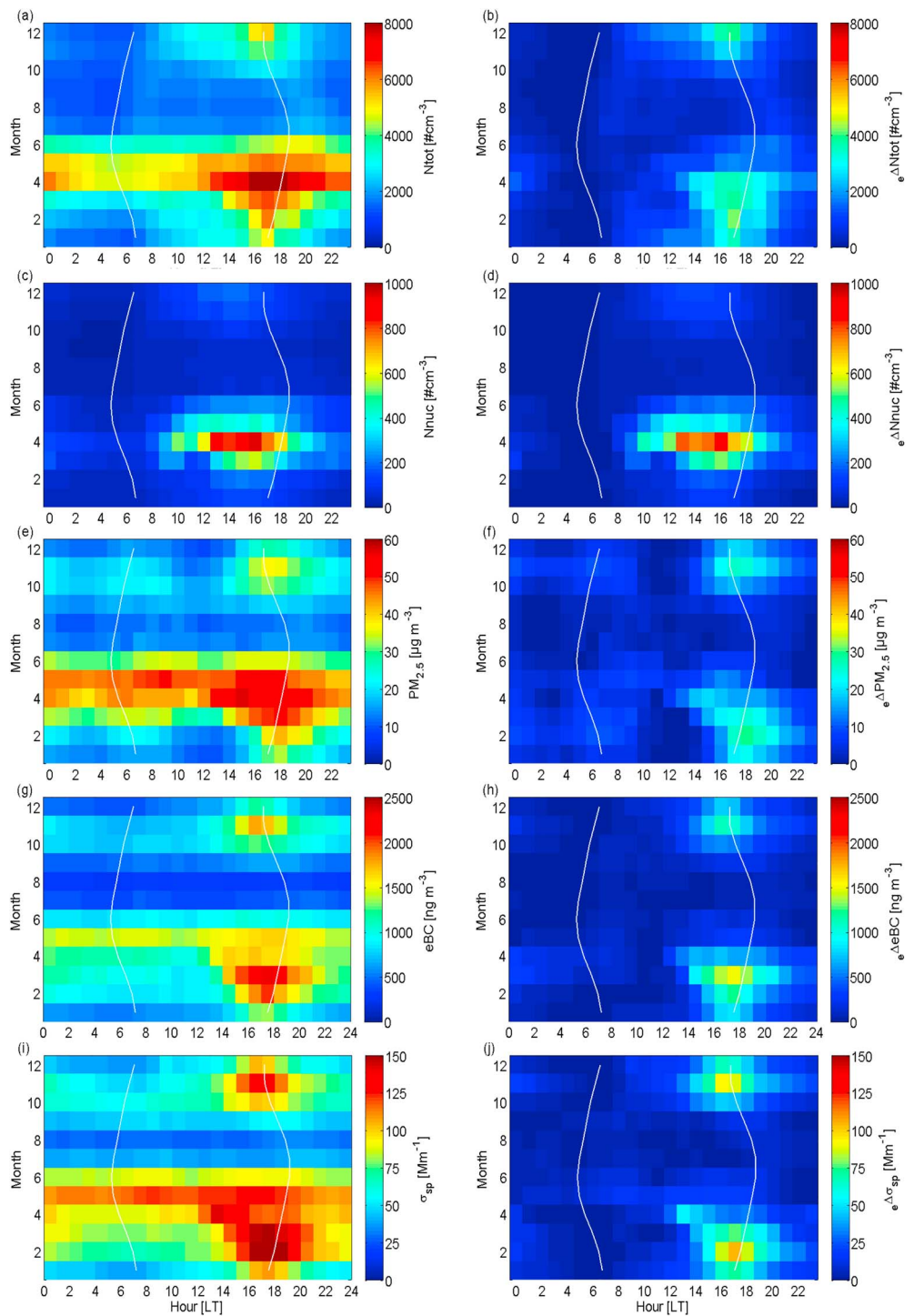


**Figure 2.** The diurnal-monthly aerosol extensive parameters representation in terms of both seasonal and diurnal variation (left column) and diurnal variation alone ( $e\Delta$ ; the minima of the diurnal values subtracted for each month [right column]). The sunrise and sunset time is shown with the white lines. eBC = equivalent black carbon.

and  $e\Delta N_{\text{nuc}}$  (Figure 2d), this shows a different behavior, being elevated only during afternoon in premonsoon, indicating new particle formation (NPF) events (Neitola et al., 2011).

In monsoon, the extensive parameter concentrations are low and constant; thus, no pronounced diurnal pattern is identified (Figure 2). Previous work (Hyvärinen, Raatikainen, Komppula, et al., 2011) has shown a

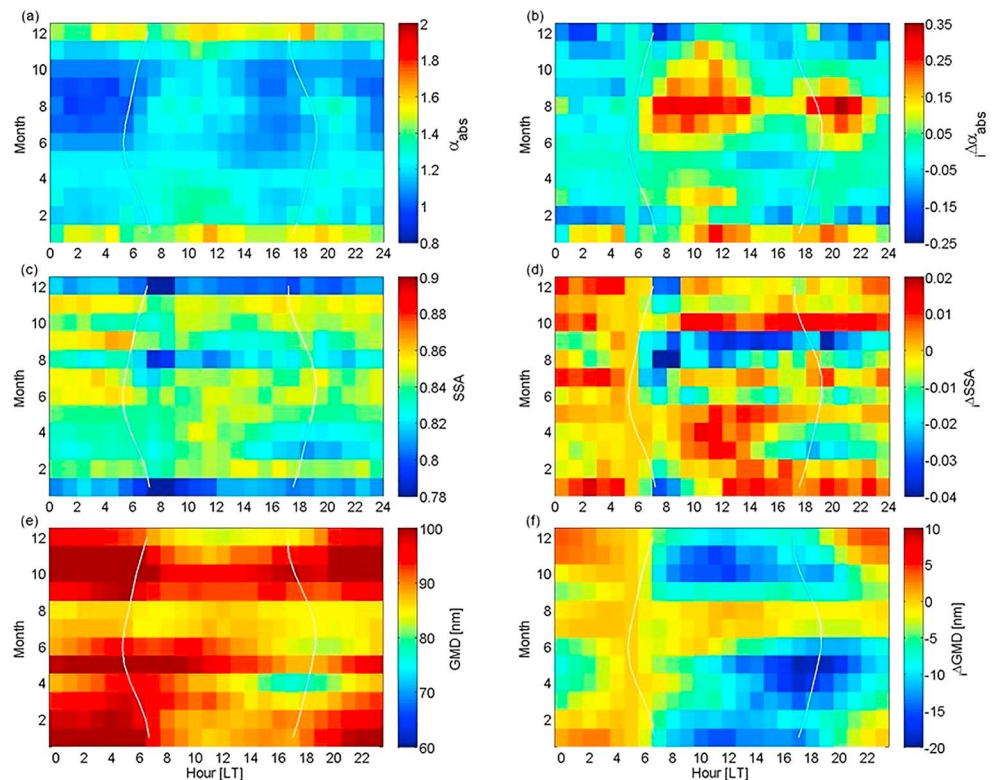


**Figure 3.** The diurnal-monthly aerosol intensive parameters representation at Mukteshwar in terms of both seasonal and diurnal variation (left column) and diurnal variation alone ( $\Delta$ ; the 5 a.m. diurnal values subtracted for each month [right column]). The sunrise and sunset time is shown with the white lines. SSA = single scattering albedo; GMD = geometric mean diameter.

decrease of 40%–75% in average concentrations of aerosol physical and optical properties during monsoon relative to the premonsoon average concentration. In postmonsoon, particle mass and number concentrations elevate again to about twofold compared to monsoon, but lower than premonsoon values. In winter, a narrow decrease in aerosol concentrations relative to postmonsoon is noticed before a peak during premonsoon (Figure 2).

Figure 3 shows the seasonal cycle of the intensive parameters ( $\alpha_{\text{abs}}$ , SSA, and GMD). The  $\alpha_{\text{abs}}$  relative to  $\Delta\alpha_{\text{abs}}$  is observed with small diurnal changes across the seasons. A high  $\alpha_{\text{abs}}$  (Figures 3a and 3b) concurrently with low SSA (Figures 3c and 3d) shows the less scattering nature of the particles in winter. Moreover, some individual (hourly average) values of SSA registered as low as  $<0.6$  in December and January, suggesting attribution of weak local or regional sources for absorbing aerosol emissions (Hyvärinen et al., 2009). In general,  $\alpha_{\text{abs}}$  in fresh biomass burning smoke can vary from 1 to 10 (depending on the combustion process; Pokhrel et al., 2016). Thus, it is difficult to infer a plausible source only based on  $\alpha_{\text{abs}}$ . But a ratio of  $N_{\text{ait}}/N_{\text{acc}}$  (supporting information Figure S8a) 1.0–1.5 times higher during the day time than the night time, together with  $\text{PM}_{2.5}/\text{PM}_{10}$  ratio between 0.8 and 0.95, can be attributed to biomass emissions, such as burning dung cakes for heating and cooking purposes in the region (Komppula et al., 2009).

The values of SSA are relatively close to each other across the seasons (0.82 to 0.84; Table 1), indicating equal changes in source strength or removal processes of absorbing and scattering types of aerosols. The values of SSA are also low, up to 0.7 in August. However, contrary to winter, in August the dispersed and low SSA values in addition to the elevated  $N_{\text{ait}}/N_{\text{acc}}$  ratio (Table 1 and supporting information Figure S8a) imply wet scavenging of aged particles (Laakso et al., 2003). Moreover, we observe a clear difference in SSA during the November and March eBC peaks. In March, the mean SSA decreases from 0.85 to 0.81 as the BC-rich aerosol reaches MUK (Figure 3c). However, in November a small increase is seen in SSA in the afternoon hours (Figure 3c).

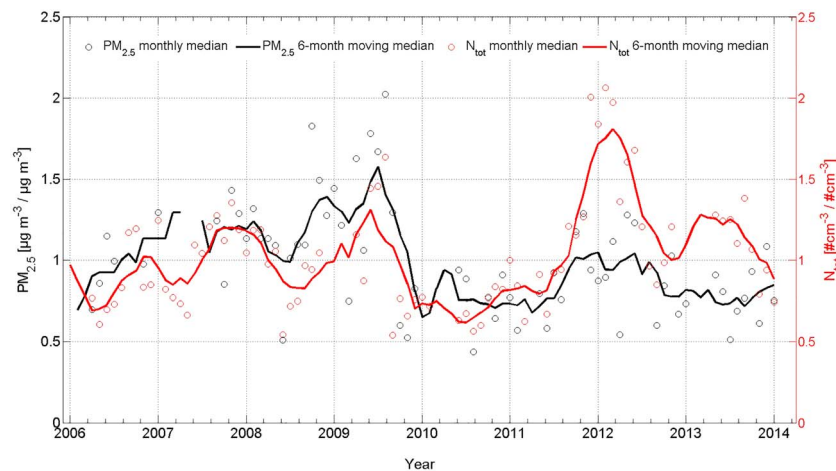


**Figure 4.** Monthly anomaly (dividing each monthly mean value by the 2005–2014 mean value for the given month) of aerosol variables. The parameters  $PM_{2.5}$  and  $N_{tot}$  are unit less.

The GMD values for MUK are little bit higher than those observed elsewhere: for example, in Siberia, over 2006–2009 measurements (Heintzenberg et al., 2011), a site relatively undisturbed by anthropogenic influences, and in central North Carolina, in a forested suburban environment during September (Ziemba et al., 2010). The nighttime values of GMD at MUK are higher than the daytime values across the months. The GMD (Figure 3e) is stable at approximately 92 nm under more stagnant conditions in the winter (Herrmann et al., 2015) and distinctly high in monsoon (Figure 3f), obviously due to wet scavenging of large particles. A high ratio of  $eBC/PM_{2.5}$  and  $N_{ait}/N_{acc}$  (Table 1 and supporting information Figure S8a) in monsoon relative to other seasons also manifests wet scavenging of large (aged) particles (Hyvärinen, Raatikainen, Komppula, et al., 2011). But a decrease in ratio of  $N_{ait}/N_{acc}$  concurrently with an increase in ratio of  $N_{acc}/N_{tot}$  (Table 1 and supporting information Figure S8b) and maxima in GMD (Figure 3e) with a distinct amplitude in  $\Delta GMD$  (Figure 3f) during postmonsoon might imply long-range transported plumes of stubble burning. The GMD is lowest at approximately 80 nm in premonsoon (specifically in April) due to NPF (supporting information Figure S10; Dal Maso et al., 2005; Komppula et al., 2009; Neitola et al., 2011). The  $\Delta GMD$  also shows distinctly very low values in early to late afternoon, especially in premonsoon.

### 3.1.2. Interannual Variability and Trend Analysis

The interannual variability in aerosol is distinct, and to get more insight into this variability, the relative deviations of monthly averaged values from the typical seasonal cycle were obtained with division of each monthly mean by respective monthly mean over the entire period 2005–2014.

The monthly anomalies in the interannual cycle are presented as an example for  $PM_{2.5}$  and  $N_{tot}$  (Figure 4). The high values of  $PM_{2.5}$  are in 2009 and  $N_{tot}$  is in both 2009 and 2012. The observed April–July monthly values of  $PM_{2.5}$  in 2009 are as high as  $80 \mu g/m^3$ , and  $N_{tot}$  is elevated to  $6,000 \text{ #cm}^{-3}$ . Again in December 2011–2012 and January–March 2012, the aerosol particle number concentration increases up to  $7,500 \text{ #cm}^{-3}$ , but  $PM_{2.5}$  remains close to or even below the seasonal mean values. In the present analysis, on average the interannual variability of both  $PM_{2.5}$  and  $N_{tot}$  is  $\pm 20\%$ .

The trend analysis at MUK shows statistically significant negative trends at 95% confidence level with slopes of  $-19 \mu g/m^3$  and of  $-23 \mu g/m^3$  in  $PM_{2.5}$  and  $PM_{10}$ , respectively, with both LMS and GLS/ARB methods. But MK analysis results in a statistically insignificant trend for both  $PM_{2.5}$  and  $PM_{10}$ . The trend analysis result of  $N_{tot}$  has a positive slope, but not statistically significant (not shown here). In summary, all other aerosol parameters observed at MUK show no statistically significant trend, either with MK or LMS analysis. The ratio of  $eBC$  to  $PM_{2.5}$  has a positive statistically significant trend of 2.44%/year corresponding to a slope of 0.06 ( $\mu g/m^3(BC/PM_{2.5})/7.7 \text{ years}$ ). However,  $eBC$  itself does not exhibit a statistically significant trend, so the observed trend in  $eBC/PM_{2.5}$  is assumed to have been caused by the negative trend in  $PM_{2.5}$ .

In general, the absence of a statistically significant trend for the other aerosol parameters can be largely attributed to the length of the time period of continuous measurements in this study. As commented in



Collaud Coen et al. (2013), trends calculated on time series shorter than 8–10 years usually present larger slopes with great confidence intervals leading to statistically insignificant trends, since the results are too much influenced by the initial and final period together with possible outliers. Interestingly, in contrast to an increase in emission loads in India (Dubash et al., 2018; Krotkov et al., 2016; Rao et al., 2016), a decreasing trend of PM is investigated at MUK, as discussed above, which corresponds to a decrease in the interannual tendency of ABL (using modeled mixing layer depth) air transport to MUK from IGP (supporting information Figure S4). However, in-depth assessment of its reasons and linkages with aerosol variability could be a future task.

On trend analysis in India, CPCB (2012) showed varying trends for PM<sub>10</sub> across 46 cities (population 1 million plus) based on their long-term (2000–2012) monitoring, while HEI (2017) indicated an increase in air pollution (PM<sub>2.5</sub>) levels since 2010. Both these results have their own limitations in terms of a robust trend analysis approach and representation of monitoring locations for all of India.

### 3.2. Factors Driving the Aerosol Variability

#### 3.2.1. Diurnal Cycle

The seasonal-diurnal plots in Figure 2 show a clear increase in all extensive aerosol parameters during late afternoon outside of the monsoon season. Raatikainen et al. (2014) identified similar patterns in aerosol patterns at MUK and used a modeled mixing depth in the plains to infer the transport of polluted air from IGP to MUK. It has previously been shown that convective mixing can transport polluted air from valleys and plains to high-altitude mountain sites (Baltensperger et al., 1997; Poltera et al., 2017; Raatikainen et al., 2014). It is known, however, that modeled mixing layer depths have uncertainties (supporting information Figure S3), especially in the mountain environment (Lehner & Rotach, 2018; Rotach et al., 2015); thus, here, due to the absence of direct measurements (Eresmaa et al., 2006) of the mixing layer depth, we use observed surface meteorological variables to determine the likely influence of boundary layer transport.

Figure 5 presents the monthly and diurnal median values in selected meteorological parameters at MUK: wind direction, wind speed, specific humidity, and solar irradiance. Outside of the monsoon season, the median wind direction (Figure 5a) has a very strong diurnal cycle, being predominantly NE-E (with 45% total contribution) during the day and N-NW (with 37% total contribution) at night. These wind directions are consistent with the alignment of the mountain ridges (Gohm et al., 2009; Pal et al., 2014; supporting information Figure S1). Figure 5 also presents the variability in winds and specific humidity, with a high variability indicating turbulence and hence an actively mixing boundary layer. The variability in wind speed and direction (Figures 5b and 5d) as well as specific humidity (Figure 5f) is much higher during the day, a consequence of the daytime convectively driven turbulent boundary layer (Stull, 1988). Strongly turbulent periods are associated with a reduction in horizontal wind speeds (Figure 5c). The strength of the turbulent mixing, indicated by the variability in each parameter, is determined by the sensible heat fluxes arising from solar irradiance (Figure 5g); good agreement between high solar irradiance and high variability in winds and specific humidity is the result of high solar irradiance generating high surface sensible heat fluxes and associated turbulent boundary layer. Note that the timing of maximum solar irradiance is, as expected, around solar noon on clear days whereas the maximum variability in winds and specific humidity is generally later in the afternoon (Prabha et al., 2012). The wind speed displays more variability than wind direction earlier in the day; however, and it is known that the boundary layer in mountainous regions has a more complex structure due to the interaction between flows at different scales (synoptic flow, valley wind, and slope flows; De Wekker & Kossmann, 2015; Ball, 1960; Tennekes, 1973; Serafin et al., 2018; Stull, 1973, 1988). At night, the variability is much lower since, in the absence of any thermal convection, any turbulent production is the result of wind shear (Serafin et al., 2018).

During the monsoon season, the diurnal pattern is heavily suppressed. In the night time the wind direction is SE (Figure 5a) since the summer monsoon circulation in India is more synoptic in scale (Kaskaoutis, Houssos, et al., 2014), and there is also more night time variability in wind speed and direction compared to other seasons. The solar irradiance at the surface is much reduced, producing weaker, surface-driven convective mixing; hence, the daytime variability in the winds and in specific humidity is not as strong as in the premonsoon and postmonsoon seasons. An additional source of turbulent mixing during the monsoon period is cloud-driven turbulence (Mehta et al., 2017).

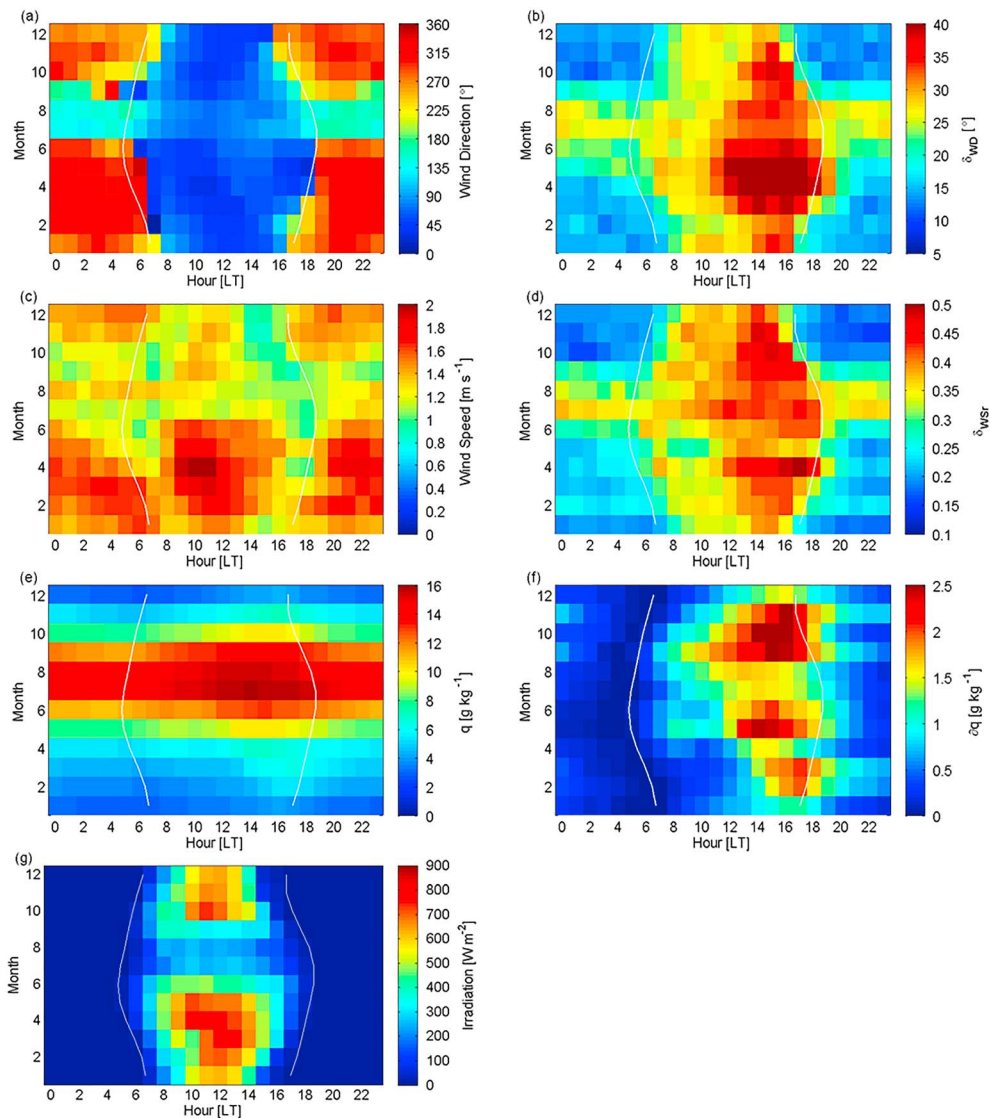


**Figure 5.** The diurnal-monthly median cycle of meteorological parameters at MUK: (a) wind direction, (b) wind direction variability (average of the absolute differences in wind direction from 1 min to the next during the given hour and represented as  $\delta_{WD}$ ), (c) wind speed, (d) wind speed variability (same way as  $\delta_{WD}$ , but in the end divided by the average wind speed of that hour and represented as  $\delta_{WSr}$ ), (e) diurnal-monthly median of specific humidity, (f) diurnal median alone (subtracting the minima of each monthly cycle from all values of the respective cycle and represented as  $\delta q$ ), (g) solar irradiation. The sunrise and sunset time is shown with the white lines.

However, the relative strength of boundary layer mixing alone is not sufficient to infer the mixing layer depth and thereby determine whether aerosol measurements at MUK are influenced by transport from the plains (IGP). The parameter  $\Phi q$  shown in Figure 6a is a much clearer indicator, as this uses the property that specific humidity is a conserved variable and is usually locally well mixed. Elevated values of  $\Phi q$  correspond very well with the observed 1.5–2 times increase in all extensive aerosol parameters at MUK seen in the early to late afternoon in Figure 2.

A weak peak in the morning is attributed to transport of air from the local valley, while the boundary layer is still growing, and the strong peak in the late afternoon relates to daytime transport of moist air masses from lower altitudes, mixed with the valley air (Figure 6a). Furthermore, the mixing layer influence is evaluated with different threshold values of  $\Phi q$  (0.25, 0.5, and 0.75) and compared to the maximum mixing depth (model based) in terms of the fraction of the days when MUK is under the influence of air from the plains



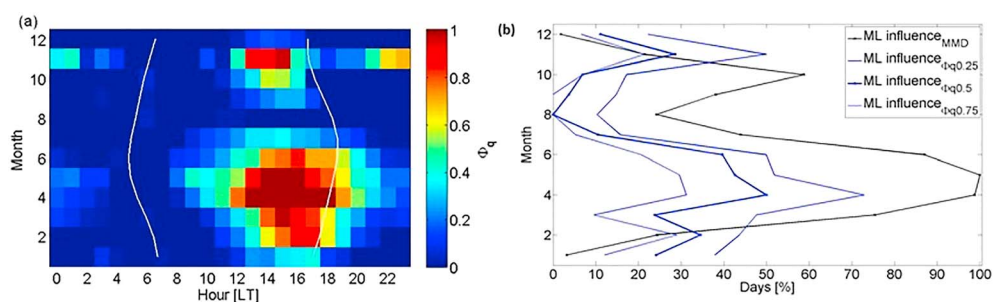


**Figure 6.** (a) Diurnal influence of atmospheric boundary layer (each hourly  $q$  value at Mukteshwar subtracted from the respective hourly  $q$  at Gual Pahari (in Indo Gangetic Plains) and divided by values at 5 a.m., represented as  $\Phi q$ ), (b) mixing layer influence as the average monthly fraction of days affected by air from Indo Gangetic Plains illustrated with maximum mixing depth and  $\Phi q$  with three threshold values (0.25, 0.5, and 0.75) shown as blue thick line in middle (0.5), and as upper (0.25), and lower (0.75). The sunrise and sunset time in (a) is shown with the white lines.

(Figure 6b), indicating the mixing of air masses dominantly in premonsoon and postmonsoon. This is in agreement with previous findings that high regional pollution can be seen in dry months at elevated sites when the boundary layer is deep enough (Collaud Coen et al., 2013).

### 3.2.2. Seasonal and Interannual Variability

Broadly, the differentiation of seasons (premonsoon and postmonsoon) in India is based on the arrival and withdrawal phases of the classified precipitation level, and that might differ across the years. One of the suggested reasons is El Niño, which delays the onset of monsoon rains by inducing enhanced subsidence, persistent during the preonset phase, and advances the withdrawal by intensifying the horizontal cold air advection (Krishna Kumar et al., 2006; Xavier et al., 2007). The months of June and September, a mix of dry and rainy periods with transitional synoptic weather conditions and synoptic scale circulation, impeded a weaker diurnal aerosol cycle (Figure 2).

Figure 4 shows exceptionally high aerosol concentration in 2009 and 2012. A delay in onset of monsoon in 2009 might be due to El Niño event (Table 2), resulting relatively high aerosol concentration. Previously, Hyvärinen, Raatikainen, Brus, et al. (2011) and Hyvärinen, Raatikainen, Komppula, et al. (2011) examined the influence of monsoon on PM and BC concentrations along with optical and physical properties at MUK and identified less of a decrease in aerosol concentration during 2009 than 2006 and 2007. The air mass trajectories in anomaly month during 2009 (supporting information Figure S7) are typical of a dry and wet period and show a seasonal corroboration to that in other years. Although, 2012 has a negative rainfall anomaly, it is below the line for drought (IITM, 2017), suggesting the anomaly was not driven primarily due

**Table 2**

Year-Wise Details of ENSO Phase, Onset, and Withdrawal of Monsoon, and Cumulative Rainfall at MUK

Year	ENSO <sup>a</sup> phase	SW monsoon onset <sup>b</sup>	SW monsoon withdrawal <sup>b</sup>	Cumulative rainfall (mm) in parenthesis (%) <sup>c</sup>		Annual cumulative rainfall (mm) <sup>d</sup>
				JJAS	JA	
2005	—	16 June	28 Sept	990 (74)	580 (43)	1,330
2006	El Niño	30 June	27 Sept	680 (75)	455 (50)	910
2007	La Niña	18 June	02 Oct	785 (60)	450 (34)	1,320
2008	—	16 June	28 Sept	1,380 (91)	775 (51)	1,510
2009	El Niño	29 June	28 Sept	900 (68)	540 (41)	1,315
2010	La Niña	05 July	28 Sept	1,490 (88)	830 (49)	1,700
2011	La Niña	20 June	26 Sept	1,220 (82)	850 (57)	1,490
2012	—	05 July	25 Sept	920 (82)	660 (60)	1,115
2013	—	15 June	15 Oct	1,190 (74)	500 (31)	1,610
2014	El Niño	01 July	04 Oct	1,000 (64)	870 (55)	1,575

Note. ENSO = El Niño–Southern Oscillation; MUK = Mukteshwar.

<sup>a</sup>All India Summer Monsoon Rainfall: <http://www.tropmet.res.in/~kolli/mol/Monsoon/frameindex.html>. <sup>b</sup>India Meteorological Department, monsoon report.

<sup>c</sup>Based on daily rainfall data (IMD, 2016; surface chemistry station at Mukteshwar); dashes refers to not classified; JJAS = June, July, August, and September (south-west SW monsoon period); JA = July and August. <sup>d</sup>Sum of JJAS (SW); and northeast (NE) monsoon (November–March); monsoon transition periods (April and May for the winter-to-summer transition, and in late September to October for the summer-to-winter transition).

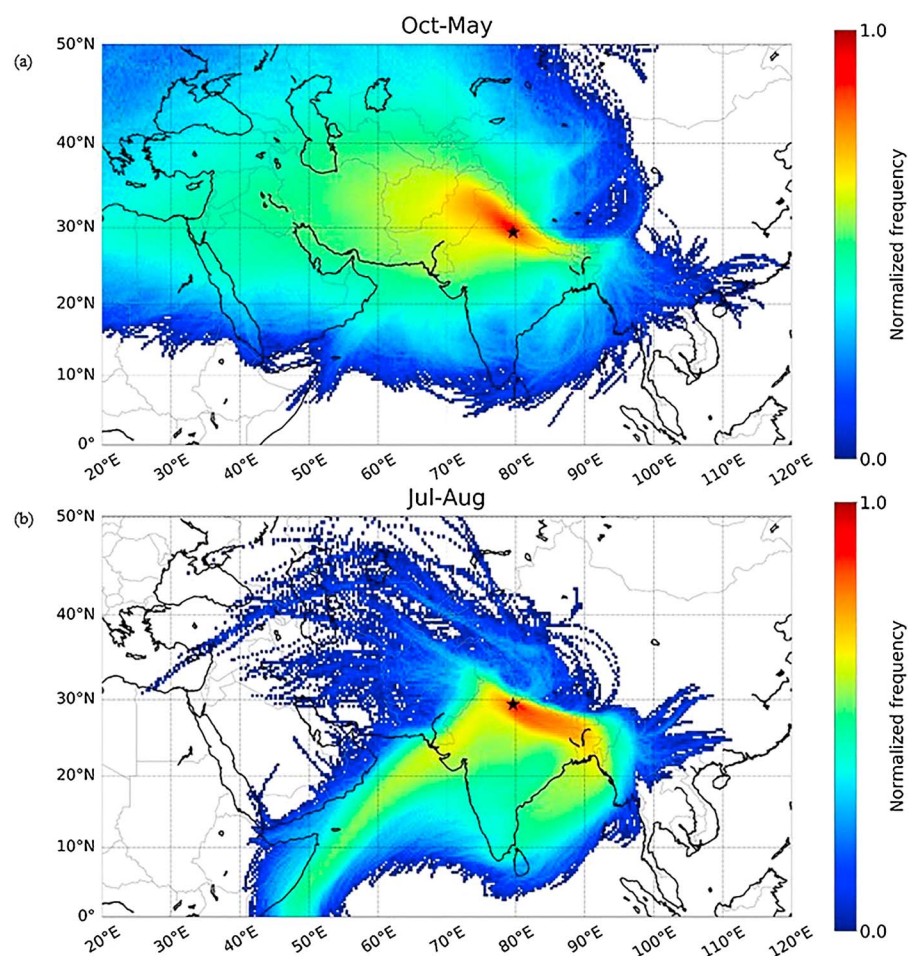


**Figure 7.** Normalized frequency of the trajectories, (a) dry period (October to May) and (b) monsoon (July and August).

to less rain. The air mass trajectories, however, are NW centered (supporting information Figure S7) and are short, with an average height above 4,000 m (range 2,500–7,500 m, not shown here; Komppula et al., 2009) along the Himalayan ridges. Therefore, for such altitudes where the aerosol layers are commonly associated with increases in sulfur dioxide ( $\text{SO}_2$ ) and CCN (cloud condensation nuclei; Clarke et al., 2013), notably when  $\text{SO}_2$  levels had been documented with increased emissions over the region (Li et al., 2017; Lu et al., 2013), this is likely to establish a linkage of the transport of such layers to MUK. However, this remains a future task for in-depth analysis. The ECHAM-HAM simulations also show an increasing pattern in  $N_{\text{tot}}$  (Figure 8). Notwithstanding, a plausible explanation of high  $N_{\text{tot}}$  and relatively low  $\text{PM}_{2.5}$  values in 2012 could not be interpreted satisfactorily through the present analysis, even though  $\text{PM}_{10}$  values are also noticed to be relatively high in March 2012 (not shown here).

In contrast to 2009 and 2012, year 2010 and 2011 have La Niña events (Table 2), hence the highest annual cumulative precipitation, suggesting the lowest aerosol concentration. In monsoon, GMD shows a dip (Figure 3) that corroborates well with earlier findings of an efficient cleansing process of particles at MUK and GP (Hyvärinen, Raatikainen, Brus, et al., 2011; Hyvärinen, Raatikainen, Komppula, et al., 2011). This is attributed to nonuniform removal of particles due to cloud processes and wet scavenging by rain, which are more efficient for larger particles scavenging.

Outside the monsoon, the IGP suffers from intense dust storms originated from the arid and desert regions of southwest Asia (Iran, Afghanistan), Arabia, and the Thar desert blanketing IGP and the Himalayan foothills (Carrico et al., 2003; Duchi et al., 2014; El-Askary et al., 2006; Kaspari et al., 2009). Figure 7 shows normalized frequency of air mass origin before arriving at MUK and traveling over large regional population centers in

the IGP region (Komppula et al., 2009) carrying a considerable amount of windblown dust and agricultural burning aerosols (Dumka et al., 2015; Kumar, Kotlarski, et al., 2015). In the dry seasons (premonsoon and postmonsoon and winter), the trajectories show air masses arriving at MUK from the northwest and southwest sectors, but in general dominated by westerly air masses (Figure 7a). In the monsoon, the air masses originate from the Arabian Sea and Bay of Bengal and arrive at MUK by moving parallel to the Himalayas (Figure 7b). The air masses ascend such that the average altitude of the trajectory is lower than the end point altitude (not shown here). The humid marine air masses travel above IGP before reaching MUK. As the wet air mass rises to the altitude of MUK, the moisture condenses and rains down, effectively removing a lot of the particles (Figure 7b). The prevailing meteorological conditions and the marine humidity are the factors that differentiate the air masses, along with the fact that during premonsoon; there is a large amount of dust at middle and upper levels of the troposphere that is also transported over MUK.

Anthropogenic emissions, both local and distant are found to lead to significant climate impacts over India (Guo et al., 2016). The emissions of  $\text{SO}_2$  (IIASA, 2011; Li et al., 2017),  $\text{NO}_x$  (Li et al., 2017), and  $\text{PM}_{2.5}$  (Guttikunda & Jawahar, 2014; HEI, 2017; Rao et al., 2016) are increasing trends in India. The  $\text{SO}_2$  and  $\text{NO}_x$  emissions are mainly released from the energy sector, road transport, and industries (IIASA, 2015). In the case of  $\text{PM}_{2.5}$ , the combustion of biomass for cooking (HEI, 2017) and emissions from coal-fired power plants (Guttikunda & Jawahar, 2014) are predominant. The emissions of BC and OM (organic matter) from the domestic sector in India show a slight decreasing or stable trend post-2010, and sulphates mainly from energy production and industries show a steep increasing trend after 2007 (IIASA, 2015).

The absolute emission strength at MUK is small in comparison to emissions over the Delhi region (supporting information Figure S6). The MUK area is often under the influence of long-range transported air masses from the IGP region, as discussed in the previous section, which results in long-range transported biomass burning aerosols (Dumka et al., 2015; Komppula et al., 2009; Kumar et al., 2011) and aged combustion-derived aerosols (Komppula et al., 2009; Raatikainen et al., 2017). The size-segregated correlation analysis reveals eBC mass contribution significantly in the size range  $> 90$  nm (supporting information Figure S9) and to that in 200–300 nm of the submicron aerosol mass spectra, suggesting attribution of aged combustion aerosol at MUK. The results are in corroboration with those observed in Hanle (Gogoi et al., 2014), a site in the western Himalayas at a higher altitude than MUK and potentially a receiver of aerosol aged further than that at MUK. Previously, Raatikainen et al. (2017) observed a similar eBC size distribution at MUK which is dominated by a mode at 210 nm during premonsoon season. The 5-day back air mass trajectories (Figure 7) also indicate long-range transported aerosol plumes at MUK. However, local anthropogenic emissions, although on a weak scale (domestic cooking and space heating), are also important. The local traffic emissions did not lead to a large aerosol load at MUK as we found no statistically robust cycle in weekday-weekend variability of extensive aerosol parameters. The values are within  $1\sigma$  (standard deviation) across the months, confirming MUK to be located away from any high traffic density roads or cities. But the remote traffic emissions from the plains cannot be ruled out.

Besides mineral dust, another major source of MUK aerosol load is crop residue burning. The increased  $\text{PM}_{2.5}$  and eBC concentrations in the afternoon hours during February–March and October–November (Figures 2e and 2g) agree with the seasonality of crop-residue burning at IGP (Kumar et al., 2011; Venkataraman et al., 2006). Domestic heating and cooking, which are also major sources of biomass burning aerosol in India (Bond et al., 2013), could have a similar signature to crop-residue burning with simultaneously increasing  $\text{PM}_{2.5}$  and eBC. However, as the observed peaks in  $\text{PM}_{2.5}$  and eBC (Figures 2f and 2h) occur during the harvesting months but not during the coldest months (December and January), we attribute these peaks to open crop-residue burning's impact on the air masses being transported from the plains to MUK. Dumka et al. (2015) observed a similar seasonality in scattering and absorption coefficients at Nainital, which was also attributed to long-range transported biomass burning aerosols. In northern India, rice residue burning is the main source of biomass burning aerosols in November, while in March, wheat residue burning prevails.

We observe a clear difference in SSA during the March and November eBC peaks. In March, the mean SSA decreases from 0.85 to 0.81 as the BC-rich aerosol reaches MUK (Figure 3c). However, in November a small increase is seen in SSA in the afternoon hours (Figure 3c). This is surprising, considering that in March, toward the end of the dry period, the amount of wind-blown dust is increasing and thus one would expect more scattering aerosol and higher SSA than in November.

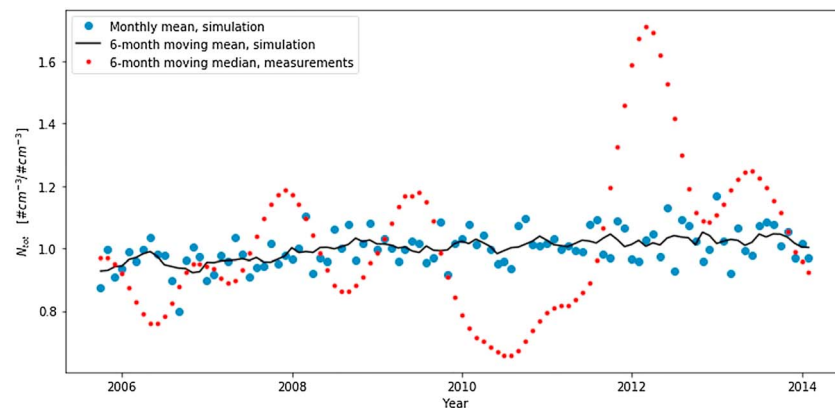


**Figure 8.** Monthly anomaly of  $N_{\text{tot}}$  in ECHAM-HAM simulations and in situ measurements at Mukteshwar.

A higher BC fraction in PM emissions from wheat residue burning compared to rice residue burning could explain the lower SSA in March. However, near-fire measurements (Ni et al., 2015; Zhang et al., 2015) do not indicate conclusive differences between the crops but report highly variable BC and  $\text{PM}_{2.5}$  emissions. Another factor that may contribute to higher SSA in November is SOA formation. In November, biogenic emissions of SOA precursors are probably higher than in March. Additionally, SOA formation in crop residue burning plumes (Vakkari et al., 2018; Yokelson et al., 2009) may make a larger contribution in November than in March. Rice is cultivated mostly  $>200$  km from MUK (Kaskaoutis, Kumar, et al., 2014), but wheat is grown also within 50–200 km of MUK; the longer transport would allow more time for in-plume SOA formation. However, this cannot be verified without further studies closer to the sources.

### 3.2.3. Modeled Aerosol Variability

In addition to observations, simulations are undertaken using two climate models with the same anthropogenic emissions but different spatial resolutions (ECHAM-HAMMOZ with a  $\sim 1.9^\circ$  resolution and the regional model REMO-HAM with a  $0.22^\circ$  resolution). These simulations are used to evaluate the models' ability to capture the observed aerosols variability (refer to section 3.1) at MUK. In both models, the model level closest to the station altitude is chosen for the comparison following Pietikäinen et al. (2012). It should be mentioned that comparing a mountain station against models with terrain following hybrid pressure based coordinates is problematic unless the model spatial resolution is very high (approximately some kilometers). In this coordinate system, the horizontal transport of aerosols is too efficient in the lowest model layers—even at times when in reality there is no transport in the layer below the MUK station. This causes overestimation in the lowest model levels of mountainous areas and is the reason why we use the height-matched level (Li et al., 2014; Zou et al., 2016, and references therein). However, the height-matched level also has some errors as the terrain following vertical coordinate levels combined with the hydrostatic model does not produce enough vertical transport at mountainous regions. This causes some artificial dilution of the concentrations, but the error is much smaller than with the lowest level approach.

Figure 8 shows the monthly mean and 6-month moving mean of  $N_{\text{tot}}$  at MUK over the period 2005–2014 in the ECHAM-HAM simulations and the observations. The anomalies are compared for the different months of the years 2005–2014. The modeling results are comparable to the corresponding observational result of anomalies of  $N_{\text{tot}}$  (Figure 4). However, since the station stays within the ABL in the model and the artificial dilution does not allow the pollution load to build up sufficiently over the plain, the height-matched model level of MUK does not receive a strong enough pollution pulse when the ABL starts to grow and encompasses MUK in the premonsoon months. We do see that the later years of the period from 2005–2014 in general have higher  $N_{\text{tot}}$  concentrations with both observational and modeling results. Additionally, many of the interannual and interseasonal variability features—for example, the peaks in early 2009 and 2012 and the low values in late 2010 and late 2011—are captured reasonably well.

On the other hand, ECHAM-HAM overestimates the measured eBC values almost throughout the analyzed period and shows a reversed seasonality with the lowest concentrations during the premonsoon. A comparison of the modeled and measured eBC concentrations at MUK with the ECHAM-HAM and



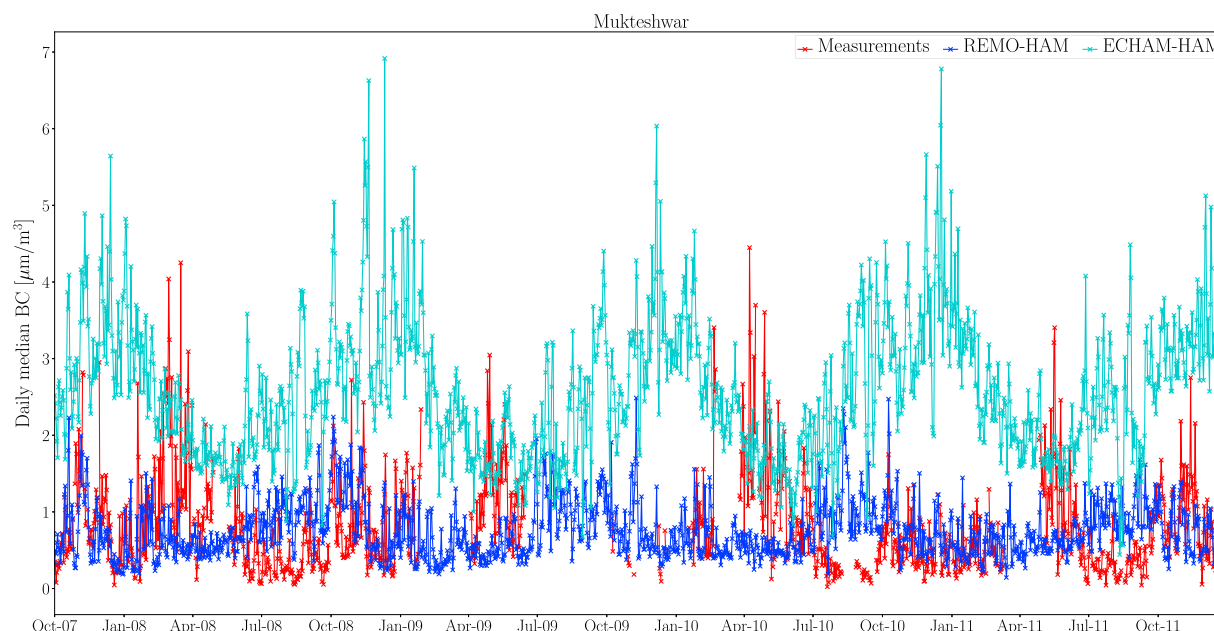


**Figure 9.** Daily median measured and modeled black carbon (BC) ground concentrations at Mukteshwar. The modeled values are from the height-matched levels.

REMO-HAM models, using the same emission inventory, is shown in Figure 9. The modeled overestimation is likely due to the coarse resolution of ECHAM-HAM, which flattens the orography and seems to artificially delay modeled precipitation so that it takes place at higher altitudes than MUK (analysis not shown). But the variability observed in measurements is captured reasonably well with the higher-resolution regional model REMO-HAM (Figure 9), apart from underestimating the measured peak concentrations during premonsoon and very slightly overestimating eBC during monsoon.

Notably, both models are able to capture the observed eBC concentrations over the IGP much more reliably (a comparison to GP is shown in supporting information Figure S11), indicating that the emission inventory does not have significant biases. This finding further indicates that transport and representation of the valley wind influence to ABL might be the main reason for the poor performance of ECHAM-HAM in modeling eBC at the mountainous MUK. Further issues include uncertainties in subgrid processes (like orographic thermal circulation) manifested in typical diurnal variation patterns, errors in model-predicted meteorology, aerosol processes, numerical model errors, and uncertainty in boundary conditions (Kumar, Barth, et al., 2015; Seibert et al., 2000). Moreover, inaccuracies in the local emissions estimations (Saikawa et al., 2017) are also possible.

#### 4. Summary and Conclusions

We present the longest time series for in situ aerosol observations at a mountain site in India. The annual and seasonal values of aerosol extensive properties at MUK show high aerosol concentrations with respect to mountain sites worldwide, but still low in comparison to rural and urban sites elsewhere in India.

Typically, the strongest variability takes place over several consecutive months, indicating a seasonal phenomenon. The interannual variability of  $PM_{2.5}$  and  $N_{tot}$  is  $\pm 20\%$ , and we attribute the variability mostly to meteorology and climate changeability, and longer-term variations in emissions. Trend analysis shows statistically significant decreasing trends of  $-2.3 \mu g m^{-3} year^{-1}$  and  $-2.7 \mu g m^{-3} year^{-1}$  for  $PM_{2.5}$  and  $PM_{10}$ , respectively. A decreasing interannual tendency for ABL air from IGP reaching MUK suggests a decrease in transport of pollution-laden air from the plains. However, investigating further this decreasing interannual tendency will be within the scope of future work.

All extensive aerosol parameters have 1.5–2 times higher values in early to late afternoon than in the night. Aerosol number concentration has a clear peak in the late afternoon and a minimum at 5:00 in the morning.

The seasonal variability is modulated due to fluctuations in different anthropogenic and natural sources, air mass flows, and/or wet scavenging. The long-range transported plumes of dust are pronounced in premonsoon, while stubble burning contributes in both premonsoon and postmonsoon. In premonsoon, notably the atmospheric NPF contributes in elevating total number concentration. The wet scavenging process in monsoon has significant influence on both extensive and intensive parameters of aerosols.

In this study, we used observed surface meteorological variables in the absence of direct measurements of the mixing layer depth to determine the likely influence of boundary layer transport to MUK. The results present the variability in winds and specific humidity, with a high variability indicating turbulence and hence an actively mixing boundary layer; however, during the monsoon season, the diurnal pattern is heavily suppressed.

But the relative strength of boundary layer mixing alone is not sufficient to infer the mixing layer depth and hence determine whether aerosol measurements at MUK are influenced by transport from the plains (IGP). Thus, in determining that variable, we use each hourly specific humidity both at MUK and GP (IGP), and referred as ( $\Phi q$ ): the fraction of MUK air originating from the plains. The parameter  $\Phi q$  is a much clearer indicator, as this uses the property that specific humidity is a conserved variable and is usually locally well mixed. Elevated values of  $\Phi q$  correspond very well with the observed 1.5–2 times increase in all extensive aerosol parameters at MUK seen in the early to late afternoon. It concludes that the water vapor proxy matches reasonably well with aerosol variability over the course of the day and across the seasons. Further, it suggests that a weak peak in aerosol concentration in the morning could be due to air from the local valley, and the strong peak in the late afternoon may be dominantly related to daytime transport of moist air masses from lower altitude, mixed with the valley air. In summary, it suggests that the mixing of air masses via vertical and horizontal transport is significant in premonsoon and postmonsoon. The monsoon season is not captured well either with water vapor proxy or modeled mixing layer depth.

The global model ECHAM-HAM simulation with nudged meteorology reproduces the interannual, interseasonal, and long-term variability of  $N_{\text{tot}}$  reasonably well. The global model is struggling with modeling eBC concentrations in the mountainous region at MUK, while the regional model REMO-HAM managed to reproduce some of the main features of the variability. Both models reproduce the concentrations well over the IGP region (e.g., GP), indicating that emissions are not highly biased in the two models. This highlights the need of sufficient resolution and correct descriptions of transport processes when investigating mountainous regions. Efforts to increase resolution and improve process descriptions ought to improve the match between observational and modeling results further in future work.

#### Acknowledgments

This work was performed with financial support by the Ministry of Foreign Affairs of Finland, project grants (264242, 268004, 284536, and 287440) received from Academy of Finland, TEKES, Finland, and DBT, India, sponsored project TAQIITA (2634/31/2015), the Centre on Excellence in Atmospheric Science funded by the Finnish Academy of Sciences (307331), European Research Council Consolidator grant project (646857), and NordForsk Nordic Center of Excellence eSTICC. V.V. is beneficiary of an AXA Research Fund postdoctoral grant. The observational data used in this study are available freely from supporting information with due co-authorship or acknowledgment. The support of D. G., T. E. R. I. was always encouraging, and R. K. H. is thankful. The authors would like to thank the FMI colleague Timo Antila for his consistent technical assistance, and staff in Mukteshwar, TERI for their routine support in maintaining the observation station over the period. Comments from three anonymous reviewers are greatly appreciated.

#### References

- Anderson, T. L., Covert, D. S., Marshall, S. F., Laucks, M. L., Charlson, R. J., Waggoner, A. P., et al. (1996). Performance characteristics of a high-sensitivity, three-wavelength, total scatter/backscatter nephelometer. *Journal of Atmospheric and Oceanic Technology*, 13(5), 967–986. [https://doi.org/10.1175/1520-0426\(1996\)013<0967:PCOAH5>2.0.CO;2](https://doi.org/10.1175/1520-0426(1996)013<0967:PCOAH5>2.0.CO;2)
- Anderson, T. L., & Ogren, J. A. (1998). Determining aerosol radiative properties using the TSI 3563 integrating Nephelometer. *Aerosol Science and Technology*, 29(1), 57–69. <https://doi.org/10.1080/02786829808965551>
- Asmi, A., Collaud Coen, M., Ogren, J. A., Andrews, E., Sheridan, P., Jefferson, A., et al. (2013). Aerosol decadal trends—Part 2: In situ aerosol particle number concentrations at GAW and ACTRIS stations. *Atmospheric Chemistry and Physics*, 13(2), 895–916. <https://doi.org/10.5194/acp-13-895-2013>
- Asmi, E., Kondratyev, V., Brus, D., Laurila, T., Lihavainen, H., Backman, J., et al. (2016). Aerosol size distribution seasonal characteristics measured in Tiksi, Russian Arctic. *Atmospheric Chemistry and Physics*, 16(3), 1271–1287. <https://doi.org/10.5194/acp-16-1271-2016>
- Baars, H., Kanitz, T., Engelmann, R., Althausen, D., Heese, B., Komppula, M., et al. (2016). An overview of the first decade of PollyNET: An emerging network of automated Raman-polarization lidars for continuous aerosol profiling. *Atmospheric Chemistry and Physics*, 16(8), 5111–5137. <https://doi.org/10.5194/acp-16-5111-2016>
- Ball, F. K. (1960). Control of inversion height by surface heating. *Quarterly Journal of the Royal Meteorological Society*, 86, 983–994.
- Baltensperger, U., Gaggeler, H. W., Jost, D. T., Lugauer, M., Schwikowski, M., Weingartner, E., & Seibert, P. (1997). Aerosol climatology at the high-alpine site Jungfraujoch, Switzerland. *Journal of Geophysical Research*, 102(D16), 19,707–19,715. <https://doi.org/10.1029/97JD00928>
- Blanco-Muriel, M., Alarcón-Padilla, D. C., López-Moratella, T., & Lara-Coira, M. (2001). Computing the solar vector. *Solar Energy*, 70, 431–441.
- Bolton, D. (1980). The Computation of Equivalent Potential Temperature. *Monthly Weather Review*, 108(7), 1046–1053. [https://doi.org/10.1175/1520-0493\(1980\)108<1046:TCEPT>2.0.CO;2](https://doi.org/10.1175/1520-0493(1980)108<1046:TCEPT>2.0.CO;2)
- Bond, T. C., Doherty, S. J., Fahey, D. W., Forster, P. M., Bertsens, T., DeAngelo, B. J., et al. (2013). Bounding the role of black carbon in the climate system: A scientific assessment. *Journal of Geophysical Research: Atmospheres*, 118, 5380–5552. <https://doi.org/10.1002/jgrd.50171>
- Carrico, C. M., Bergin, M. H., Shrestha, A. B., Dibb, J. E., Gomes, L., & Harris, J. M. (2003). The importance of carbon and mineral dust to seasonal aerosol properties in the Nepal Himalaya. *Atmospheric Environment*, 37(20), 2811–2824. [https://doi.org/10.1016/S1352-2310\(03\)00197-3](https://doi.org/10.1016/S1352-2310(03)00197-3)
- Census of India (2011). *Provisional population totals: rural-urban distribution Volume 2, Issue 1 of Census of India, 2011, India*. India: Office of the Registrar General & Census Commissioner.



- Chakraborty, A., Bhattu, D., Gupta, T., Tripathi, S. N., & Canagaratna, M. R. (2015). Real-time measurements of ambient aerosols in a polluted Indian city: Sources, characteristics, and processing of organic aerosols during foggy and nonfoggy periods. *Journal of Geophysical Research: Atmospheres*, 120, 9006–9019. <https://doi.org/10.1002/2015JD023419>
- Charlson, R. J., Schwartz, S. E., Hales, J. M., Cess, R. D., Coakley, J. A., Hansen, J. E., & Hofmann, D. J. (1992). Climate forcing by anthropogenic aerosols. *Science*, 255(5043), 423–430. <https://doi.org/10.1126/science.255.5043.423>
- Clarke, A. D., Freitag, S., Simpson, R. M. C., Hudson, J. G., Howell, S. G., Brekhovskikh, V. L., et al. (2013). Free troposphere as a major source of CCN for the equatorial Pacific boundary layer: Long-range transport and teleconnections. *Atmospheric Chemistry and Physics*, 13(15), 7511–7529. <https://doi.org/10.5194/acp-13-7511-2013>
- Collaud Coen, M., Andrews, E., Aliaga, D., Andrade, M., Angelov, H., Bukowiecki, N., et al. (2018). Identification of topographic features influencing aerosol observations at high altitude stations. *Atmospheric Chemistry and Physics*, 18(16), 12,289–12,313. <https://doi.org/10.5194/acp-18-12289-2018>
- Collaud Coen, M., Andrews, E., Asmi, A., Baltensperger, U., Bukowiecki, N., Day, D., et al. (2013). Aerosol decadal trends – Part 1: In situ optical measurements at GAW and IMPROVE stations. *Atmospheric Chemistry and Physics*, 13(2), 869–894. <https://doi.org/10.5194/acp-13-869-2013>
- Collaud Coen, M., Weingartner, E., Apituley, A., Ceburnis, D., Fierz-Schmidhauser, R., Flentje, H., et al. (2010). Minimizing light absorption measurement artifacts of the Aethalometer: Evaluation of five correction algorithms. *Atmospheric Measurement Techniques*, 3(2), 457–474. <https://doi.org/10.5194/amt-3-457-2010>
- Collaud Coen, M., Weingartner, E., Nyeki, S., Cozic, J., Henning, S., Verheggen, B., et al. (2007). Long-term trend analysis of aerosol variables at the high-alpine site Jungfraujoch. *Journal of Geophysical Research*, 112, D13213. <https://doi.org/10.1029/2006JD007995>
- CPCB (2010). *Air quality monitoring, emission inventory and source apportionment study for Indian Cities*. New Delhi, India: Central Pollution Control Board, Government of India.
- CPCB. (2012). National ambient air quality status and trends in India –2010; NAAQMS/35/2011–2012.
- Dal Maso, M., Kulmala, M., Riipinen, I., Wagner, R., Hussein, T., Aalto, P. P., & Lehtinen, K. E. J. (2005). Formation and growth of fresh atmospheric aerosols: Eight years of aerosol size distribution data from SMEAR II, Hyytiälä, Finland. *Boreal Environment Research*, 10, 323–336.
- De Wekker, S. F. J., & Kossmann, M. (2015). Convective boundary layer heights over mountainous terrain—A review of concepts. *Frontiers of Earth Science*, 3, 77. <https://doi.org/10.3389/feart.2015.00077>
- DeCarlo, P. F., Slowik, J. G., Worsnop, D. R., Davidovits, P., & Jimenez, J. L. (2004). Particle morphology and density characterization by combined mobility and aerodynamic diameter measurements. Part 1: Theory. *Aerosol Science and Technology*, 38(12), 1185–1205. <https://doi.org/10.1080/027868290903907>
- Dee, D. P., Uppala, S. M., Simmons, A. J., Berrisford, P., Poli, P., Kobayashi, S., et al. (2011). The ERA-interim reanalysis: Configuration and performance of the data assimilation system. *Quarterly Journal of the Royal Meteorological Society*, 137(656), 553–597. <https://doi.org/10.1002/qj.828>
- Di Girolamo, L., Bond, T. C., Bramer, D., Diner, D. J., Fettingner, F., Kahn, R. A., et al. (2004). Analysis of Multi-angle Imaging SpectroRadiometer (MISR) aerosol optical depths over greater India during winter 2001–2004. *Geophysical Research Letters*, 31, L23115. <https://doi.org/10.1029/2004GL021273>
- Draxler, R. R., & Hess, G. D. (1998). An overview of the HYSPLIT\_4 modelling system for trajectories, dispersion, and deposition. *Australian Meteorological Magazine*, 47, 295–308.
- Dubash, N. K., Khosla, R., Rao, N. D., & Bhardwaj, A. (2018). India's energy and emissions future: An interpretive analysis of model scenarios. *Environmental Research Letters*, 13(7), 074018. <https://doi.org/10.1088/1748-9326/aacc74>
- Duchi, R., Cristofanelli, P., Marinoni, A., Bourcier, L., Laj, P., & Calzolari, F. (2014). Synoptic-scale dust transport events in the southern Himalaya. *Aeolian Research*, 13, 51–57. <https://doi.org/10.1016/j.aeolia.2014.03.008>
- Dumka, U. C., Kaskaoutis, D. G., Srivastava, M. K., & Devara, P. C. S. (2015). Scattering and absorption properties of near-surface aerosol over Gangetic–Himalayan region: The role of boundary-layer dynamics and long-range transport. *Atmospheric Chemistry and Physics*, 15(3), 1555–1572. <https://doi.org/10.5194/acp-15-1555-2015>
- El-Askary, H., Gautam, R., Singh, R. P., & Kafatos, M. (2006). Dust storms detection over the Indo-Gangetic basin using multi sensor data. *Advances in Space Research*, 37(4), 728–733. <https://doi.org/10.1016/j.asr.2005.03.134>
- Eresmaa, N., Karppinen, A., Joffe, S. M., Räsänen, J., & Talvitie, H. (2006). Mixing height determination by ceilometer. *Atmospheric Chemistry and Physics*, 6(6), 1485–1493. <https://doi.org/10.5194/acp-6-1485-2006>
- Fleming, Z. L., Monks, P. S., & Manning, A. J. (2012). Review: Untangling the influence of air-mass history in interpreting observed atmospheric composition. *Atmospheric Research*, 104–105, 1–39. <https://doi.org/10.1016/j.atmosres.2011.09.009>
- Ganguly, D., Jayaraman, A., Rajesh, T. A., & Gadgavi, H. (2006). Winter-time aerosol properties during foggy and nonfoggy days over urban center Delhi and their implications for shortwave radiative forcing. *Journal of Geophysical Research*, 111, D15217. <https://doi.org/10.1029/2005JD007029>
- Gautam, R., Hsu, N. C., Kafatos, M., & Tsay, S.-C. (2007). Influences of winter haze on fog/low cloud over the Indo-Gangetic plains. *Journal of Geophysical Research*, 112, D05207. <https://doi.org/10.1029/2005JD007036>
- Gautam, R., & Singh, M. K. (2018). Urban heat island over Delhi punches holes in widespread fog in the Indo-Gangetic Plains. *Geophysical Research Letters*, 45, 1114–1121. <https://doi.org/10.1002/2017GL076794>
- Gogoi, M. M., Moorthy, K. K., Kompalli, S. K., Chaubey, J. P., Babu, S. S., Manoj, M. R., et al. (2014). Physical and optical properties of aerosols in a free tropospheric environment: Results from long-term observations over western trans-Himalayas. *Atmospheric Environment*, 84, 262–274. <https://doi.org/10.1016/j.atmosenv.2013.11.029>
- Gohm, A., Harnisch, F., Vergeiner, J., Obleitner, F., Schnitzhofer, R., Hansel, A., et al. (2009). Air pollution transport in an Alpine Valley: Results from airborne and ground-based observations. *Boundary-Layer Meteorology*, 131(3), 441–463. <https://doi.org/10.1007/s10546-009-9371-9>
- Guo, L., Turner, A. G., & Highwood, E. J. (2016). Local and Remote Impacts of Aerosol Species on Indian Summer Monsoon Rainfall in a GCM. *Journal of Climate*, 29(19), 6937–6955. <https://doi.org/10.1175/JCLI-D-15-0728.1>
- Guttikunda, S. K., & Jawahar, P. (2014). Atmospheric emissions and pollution from the coal-fired thermal power plants in India. *Atmospheric Environment*, 92, 449–460. <https://doi.org/10.1016/j.atmosenv.2014.04.057>
- HEI (2017). State of global air, A special report on global exposure to air pollution and its disease burden. [https://www.stateofglobalair.org/sites/default/files/SOGA2017\\_report.pdf](https://www.stateofglobalair.org/sites/default/files/SOGA2017_report.pdf)
- Heintzenberg, J., Birmili, W., Otto, R., Andreae, M. O., Mayer, J.-C., Chi, X., & Panov, A. (2011). Aerosol particle number size distributions and particulate light absorption at the ZOTTO tall tower (Siberia), 2006–2009. *Atmospheric Chemistry and Physics*, 11(16), 8703–8719. <https://doi.org/10.5194/acp-11-8703-2011>

- Henriksson, S. V., Pietikäinen, J.-P., Hyvärinen, A.-P., Räisänen, P., Kupiainen, K., Tonttila, J., et al. (2014). Spatial distributions and seasonal cycles of aerosol climate effects in India seen in a global climate–aerosol model. *Atmospheric Chemistry and Physics*, 14(18), 10,177–10,192. <https://doi.org/10.5194/acp-14-10177-2014>
- Herrmann, E., Weingartner, E., Henne, S., Vuilleumier, L., Bukowiecki, N., Steinbacher, M., et al. (2015). Analysis of long-term aerosol size distribution data from Jungfraujoch with emphasis on free tropospheric conditions, cloud influence, and air mass transport. *Journal of Geophysical Research: Atmospheres*, 120, 9459–9480. <https://doi.org/10.1002/2015JD023660>
- Hooda, R. K., Hyvärinen, A.-P., Vestenius, M., Gilardoni, S., Sharma, V. P., Vignati, E., et al. (2016). Atmospheric aerosols local-regional discrimination for a semi-urban area in India. *Atmospheric Research*, 168, 13–23. <https://doi.org/10.1016/j.atmosres.2015.08.014>
- Hyvärinen, A.-P., Lihavainen, H., Komppula, M., Panwar, T. S., Sharma, V. P., Hooda, R. K., & Viisanen, Y. (2010). Aerosol measurements at the Gual Pahari EUCAARI station: Preliminary results from in situ measurements. *Atmospheric Chemistry and Physics*, 10(15), 7241–7252. <https://doi.org/10.5194/acp-10-7241-2010>
- Hyvärinen, A.-P., Lihavainen, H., Komppula, M., Sharma, V. P., Kerminen, V.-M., Panwar, T. S., & Viisanen, Y. (2009). Continuous measurements of optical properties of atmospheric aerosols in Mukteshwar, northern India. *Journal of Geophysical Research*, 114, D08207. <https://doi.org/10.1029/2008JD011489>
- Hyvärinen, A.-P., Raatikainen, T., Brus, D., Komppula, M., Panwar, T. S., Hooda, R. K., et al. (2011). Effect of the summer monsoon on aerosols at two measurement stations in northern India – Part 1: PM and BC concentrations. *Atmospheric Chemistry and Physics*, 11(16), 8271–8282. <https://doi.org/10.5194/acp-11-8271-2011>
- Hyvärinen, A.-P., Raatikainen, T., Komppula, M., Mielonen, T., Sundström, A.-M., Brus, D., et al. (2011). Effect of the summer monsoon on aerosols at two measurement stations in northern India – Part 2: Physical and optical properties. *Atmospheric Chemistry and Physics*, 11(16), 8283–8294. <https://doi.org/10.5194/acp-11-8283-2011>
- Hyvärinen, A.-P., Vakkari, V., Laakso, L., Hooda, R. K., Sharma, V. P., Panwar, T. S., et al. (2013). Correction for a measurement artifact of the multi-angle absorption photometer (MAAP) at high black carbon mass concentration levels. *Atmospheric Measurement Techniques*, 6(1), 81–90. <https://doi.org/10.5194/amt-6-81-2013>
- International Institute for Applied Systems Analysis (IIASA) (2011). World outlook report, Emissions of air pollutants for the world energy outlook 2011 energy scenarios, <http://pure.iiasa.ac.at/9766/1/XO-11-028.pdf>. (Accessed in Mar 2017.)
- International Institute for Applied Systems Analysis (IIASA) (2015). [http://www.iiasa.ac.at/web/home/research/researchPrograms/air/Global\\_emissions.html](http://www.iiasa.ac.at/web/home/research/researchPrograms/air/Global_emissions.html). (accessed in June 2015.)
- Indian Institute of Tropical Meteorology (IITM) (2017). All India Summer Monsoon Rainfall (AISMR) <http://www.tropmet.res.in/~kolli/mol/Monsoon/frameindex.html>. (accessed in Jan 2017.)
- India Meteorological Department (IMD) (2016). Personal communication.
- Intergovernmental Panel on Climate Change (2007). Climate change 2007: The physical science basis. In S. Solomon, D. Qin, M. Manning, Z. Chen, M. Marquis, K. B. Averyt, et al. (Eds.), *Contribution of Working Group I to the Fourth Assessment Report of the Intergovernmental Panel on Climate Change* (pp. 153–171). Cambridge, UK and New York: Cambridge University Press.
- Intergovernmental Panel on Climate Change (2013). Climate change 2013: The physical science basis. In T. F. Stocker, D. Qin, G.-K. Plattner, M. Tignor, S. K. Allen, J. Boschung, A. Nauels, Y. Xia, V. Bex, & P. M. Midgley (Eds.), *Contribution of Working Group I to the Fifth Assessment Report of the IPCC* (pp. 675–686). Cambridge, United Kingdom: Cambridge University Press.
- Indian Space Research Organisation (ISRO) (2004). Special Land Based Campaign on Aerosols. <http://www.isro.gov.in/update/04-feb-2004/special-atmospheric-aerosol-campaign-launched>. (accessed in Jan 2017.)
- Kanamitsu, M. (1989). Description of the NMC Global Data Assimilation and Forecast System. *Weather and Forecasting*, 4(3), 335–342. <https://doi.org/10.1175/1520-0434>
- Kaskaoutis, D. G., Houssos, E. E., Goto, D., Bartzokas, A., Nastos, P. T., Sinha, P. R., et al. (2014). Synoptic weather conditions and aerosol episodes over Indo-Gangetic Plains, India. *Climate Dynamics*, 43(9–10), 2313–2331. <https://doi.org/10.1007/s00382-014-2055-2>
- Kaskaoutis, D. G., Kumar, S., Sharma, D., Singh, R. P., Kharol, S. K., Sharma, M., et al. (2014). Effects of crop residue burning on aerosol properties, plume characteristics, and long-range transport over northern India. *Journal of Geophysical Research: Atmospheres*, 119, 5424–5444. <https://doi.org/10.1002/2013JD021357>
- Kaspari, S., Mayewski, P. A., Handley, M., Kang, S., Hou, S., Sneed, S., et al. (2009). A high-resolution record of atmospheric dust composition and variability since A.D. 1650 from a Mount Everest ice core. *Journal of Climate*, 22(14), 3910–3925. <https://doi.org/10.1175/2009JCLI2518.1>
- Komppula, M., Lihavainen, H., Hyvärinen, A.-P., Kerminen, V.-M., Panwar, T. S., Sharma, V. P., & Viisanen, Y. (2009). Physical properties of aerosol particles at a Himalayan background site in India. *Journal of Geophysical Research*, 114, D12202. <https://doi.org/10.1029/2008JD011007>
- Komppula, M., Mielonen, T., Arola, A., Korhonen, K., Lihavainen, H., Hyvärinen, A.-P., et al. (2012). Technical note: One year of Raman-lidar measurements in Gual Pahari EUCAARI site close to New Delhi in India – Seasonal characteristics of the aerosol vertical structure. *Atmospheric Chemistry and Physics*, 12(10), 4513–4524. <https://doi.org/10.5194/acp-12-4513-2012>
- Kotamarthi, V. R. (2010). Ganges valley aerosol experiment: Science and operations plan. DOE/SC-ARM-10-019, available at: <http://www.arm.gov/publications/programdocs/doe-sc-arm-10-019.pdf?id=25>. (Accessed on 10 August 2016).
- Kowol-Santen, J., Beekmann, M., Schmitgen, S., & Dewey, K. (2001). Tracer analysis of transport from the boundary layer to the free troposphere. *Geophysical Research Letters*, 28(15), 2907–2910. <https://doi.org/10.1029/2001GL012908>
- Krishna Kumar, K., Rajagopalan, B., Hoerling, M., Bates, G., & Cane, M. (2006). Unraveling the mystery of Indian monsoon failure during El Niño. *Science*, 314(5796), 115–119. <https://doi.org/10.1126/science.1131152>
- Krotkov, N. A., McLinden, C. A., Li, C., Lamsal, L. N., Celarier, E. A., Marchenko, S. V., et al. (2016). Aura OMI observations of regional SO<sub>2</sub> and NO<sub>2</sub> pollution changes from 2005 to 2015. *Atmospheric Chemistry and Physics*, 16(7), 4605–4629. <https://doi.org/10.5194/acp-16-4605-2016>
- Kumar, P., Kotlarski, S., Moseley, C., Sieck, K., Frey, H., Stoffel, M., & Jacob, D. (2015). Response of Karakoram-Himalayan glaciers to climate variability and climatic change: A regional climate model assessment. *Geophysical Research Letters*, 42, 1818–1825. <https://doi.org/10.1002/2015GL063392>
- Kumar, R., Barth, M. C., Pfister, G. G., Nair, V. S., Ghude, S. D., & Ojha, N. (2015). What controls the seasonal cycle of black carbon aerosols in India? *Journal of Geophysical Research: Atmospheres*, 120, 7788–7812. <https://doi.org/10.1002/2015JD023298>
- Kumar, R., Naja, M., Sathesh, S. K., Ojha, N., Joshi, H., Sarangi, T., et al. (2011). Influences of the springtime northern Indian biomass burning over the Central Himalayas. *Journal of Geophysical Research*, 116, D19302. <https://doi.org/10.1029/2010JD015509>
- Kumar, S., Kumar, S., Kaskaoutis, D. G., Singh, R. P., Singh, R. K., Mishra, A. K., et al. (2015). Meteorological, atmospheric and climatic perturbations during major dust storms over Indo-Gangetic Basin. *Aeolian Research*, 17, 15–31. <https://doi.org/10.1016/j.aeolia.2015.01.006>
- Laakso, L., Hussein, T., Aarnio, P., Komppula, M., Hiltunen, V., Viisanen, Y., & Kulmala, M. (2003). Diurnal and annual characteristics of particle mass and number concentrations in urban, rural and Arctic environments in Finland. *Atmospheric Environment*, 37(19), 2629–2641. [https://doi.org/10.1016/S1352-2310\(03\)00206-1](https://doi.org/10.1016/S1352-2310(03)00206-1)

- Lehner, M., & Rotach, M. W. (2018). Current challenges in understanding and predicting transport and exchange in the atmosphere over mountainous terrain. *Atmosphere*, 9(7), 276. <https://doi.org/10.3390/atmos9070276>
- Lelieveld, J., Crutzen, P. J., Ramanathan, V., Andreae, M. O., Brenninkmeijer, C. A. M., Campos, T., et al. (2001). The Indian Ocean experiment: Widespread air pollution from South and Southeast Asia. *Science*, 291(5506), 1031–1036. <https://doi.org/10.1126/science.1057103>
- Li, C., McLinden, C., Fioletov, V., Krotkov, N., Carn, S., Joiner, J., et al. (2017). India is overtaking China as the World's largest emitter of anthropogenic sulfur dioxide. *Scientific Reports*, 7(1), 14304. <https://doi.org/10.1038/s41598-017-14639-8>
- Li, Y., Wang, B., Wang, D., Li, J., & Dong, L. (2014). An orthogonal terrain-following coordinate and its preliminary tests using 2-D idealized advection experiments. *Geoscientific Model Development*, 7(4), 1767–1778. <https://doi.org/10.5194/gmd-7-1767-2014>
- Lu, Z., Streets, D. G., de Foy, B., & Krotkov, N. A. (2013). Ozone monitoring instrument observations of interannual increases in SO<sub>2</sub> emissions from Indian coal-fired power plants during 2005–2012. *Environmental Science & Technology*, 47(24), 13,993–14,000. <https://doi.org/10.1021/es4039648>
- Matt, F. N., Burkhart, J. F., & Pietikäinen, J.-P. (2016). Modelling hydrologic impacts of light absorbing aerosol deposition on snow at the catchment scale. *Hydrology and Earth System Sciences*, 2016, 1–35. <https://doi.org/10.5194/hess-2016-551>
- Mehta, S. K., Ratnam, M. V., Sunilkumar, S. V., Rao, D. N., & Krishna Murthy, B. V. (2017). Diurnal variability of the atmospheric boundary layer height over a tropical station in the Indian monsoon region. *Atmospheric Chemistry and Physics*, 17(1), 531–549. <https://doi.org/10.5194/acp-17-531-2017>
- Messerli, B., & Ives, J. (Eds) (1997). *Mountains of the world: A global priority*. New York, London: Parthenon.
- Meybeck, M., Green, P., & Vörösmarty, C. (2001). A new typology for mountains and other relief classes. *Mountain Research and Development*, 21(1), 34–45. [https://doi.org/10.1659/0276-4741\(2001\)021\[0034:ANTFMA\]2.0.CO;2](https://doi.org/10.1659/0276-4741(2001)021[0034:ANTFMA]2.0.CO;2)
- Moorthy, K., Niranjana, K., Narasimhamurthy, B., Agashe, V. V., & Krishna Murthy, B. V. (1999). Aerosol climatology over India: 1. ISRO GBP MWR Network and database, ISRO-GBP Sci. Rep. 03-99, Indian Space Res. Organ., Bangalore.
- Moorthy, K. K., Sathesh, S. K., Sarin, M. M., & Panday, A. K. (2016). South Asian aerosols in perspective: Preface to the special issue. *Atmospheric Environment*, 125, 307–311. <https://doi.org/10.1016/j.atmosenv.2015.10.073>
- Moosmüller, H., & Arnott, W. P. (2003). Angular truncation errors in integrating nephelometry. *Review of Scientific Instruments*, 74(7), 3492–3501. <https://doi.org/10.1063/1.1581355>
- Müller, T. (2015). Development of correction factors for Aethalometers AE31 and AE33, ACTRIS-2 WP3 Workshop, Athens 10–12 November 2015.
- Müller, T., Henzing, J. S., de Leeuw, G., Wiedensohler, A., Alastuey, A., Angelov, H., et al. (2011). Characterization and intercomparison of aerosol absorption photometers: Result of two intercomparison workshops. *Atmospheric Measurement Techniques*, 4(2), 245–268. <https://doi.org/10.5194/amt-4-245-2011>
- Neitola, K., Asmi, E., Komppula, M., Hyvärinen, A.-P., Raatikainen, T., Panwar, T. S., et al. (2011). New particle formation infrequently observed in Himalayan foothills – Why? *Atmospheric Chemistry and Physics*, 11(16), 8447–8458. <https://doi.org/10.5194/acp-11-8447-2011>
- Ni, H., Han, Y., Cao, J., Chen, L.-W. A., Tian, J., Wang, X., & Wang, P. (2015). Emission characteristics of carbonaceous particles and trace gases from open burning of crop residues in China. *Atmospheric Environment*, 123, 399–406. <https://doi.org/10.1016/j.atmosenv.2015.05.007>
- Nieminen, T., Kerminen, V.-M., Petäjä, T., Aalto, P. P., Arshinov, M., Asmi, E., et al. (2018). Global analysis of continental boundary layer new particle formation based on long-term measurements. *Atmospheric Chemistry and Physics*, 18(19), 14,737–14,756. <https://doi.org/10.5194/acp-18-14737-2018>
- Ohara, T., Akimoto, H., Kurokawa, J., Horii, N., Yamaji, K., Yan, X., & Hayasaka, T. (2007). An Asian emission inventory of anthropogenic emission sources for the period 1980–2020. *Atmospheric Chemistry and Physics*, 7(16), 4419–4444. <https://doi.org/10.5194/acp-7-4419-2007>
- Pal, S., Lee, T. R., Phelps, S., & De Wekker, S. F. J. (2014). Impact of atmospheric boundary layer depth variability and wind reversal on the diurnal variability of aerosol concentration at a valley site. *Science of the Total Environment*, 496, 424–434. <https://doi.org/10.1016/j.scitotenv.2014.07.067>
- Panwar, T. S., Hooda, R. K., Lihavainen, H., Hyvärinen, A. P., Sharma, V. P., & Viisanen, Y. (2013). Atmospheric aerosols at a regional background Himalayan site—Mukteshwar, India. *Environmental Monitoring and Assessment*, 185(6), 4753–4764. <https://doi.org/10.1007/s10661-012-2902-8>
- Pietikäinen, J.-P., Kupiainen, K., Klimont, Z., Makkonen, R., Korhonen, H., Karinkanta, R., et al. (2015). Impacts of emission reductions on aerosol radiative effects. *Atmospheric Chemistry and Physics*, 15(10), 5501–5519. <https://doi.org/10.5194/acp-15-5501-2015>
- Pietikäinen, J.-P., O'Donnell, D., Teichmann, C., Karstens, U., Pfeifer, S., Kazil, J., et al. (2012). The regional aerosol-climate model REMO-HAM. *Geoscientific Model Development*, 5(6), 1323–1339. <https://doi.org/10.5194/gmd-5-1323-2012>
- Pokhrel, R. P., Wagner, N. L., Langridge, J. M., Lack, D. A., Jayarathne, T., Stone, E. A., et al. (2016). Parameterization of single-scattering albedo (SSA) and absorption Ångström exponent (AAE) with EC/OC for aerosol emissions from biomass burning. *Atmospheric Chemistry and Physics*, 16(15), 9549–9561. <https://doi.org/10.5194/acp-16-9549-2016>
- Poltera, Y., Martucci, G., Collaud Coen, M., Hervö, M., Emmenegger, L., Henne, S., et al. (2017). PathfinderTURB: An automatic boundary layer algorithm. Development, validation and application to study the impact on in situ measurements at the Jungfraujoch. *Atmospheric Chemistry and Physics*, 17(16), 10,051–10,070. <https://doi.org/10.5194/acp-17-10051-2017>
- Prabha, T. V., Karipot, A., Axisa, D., Kumari, B. P., Mahes Kumar, R. S., Konwar, M., et al. (2012). Scale interactions near the foothills of Himalayas during CAIPEEX. *Journal of Geophysical Research*, 117, D10203. <https://doi.org/10.1029/2011JD016754>
- Raatikainen, T., Brus, D., Hooda, R. K., Hyvärinen, A.-P., Asmi, E., Sharma, V. P., et al. (2017). Size-selected black carbon mass distributions and mixing state in polluted and clean environments of northern India. *Atmospheric Chemistry and Physics*, 17(1), 371–383. <https://doi.org/10.5194/acp-17-371-2017>
- Raatikainen, T., Hyvärinen, A.-P., Hatakka, J., Panwar, T. S., Hooda, R. K., Sharma, V. P., & Lihavainen, H. (2014). The effect of boundary layer dynamics on aerosol properties at the indo-Gangetic plains and at the foothills of the Himalayas. *Atmospheric Environment*, 89, 548–555. <https://doi.org/10.1016/j.atmosenv.2014.02.058>
- Rajput, P., Sarin, M. M., Sharma, D., & Singh, D. (2014). Characteristics and emission budget of carbonaceous species from postharvest agricultural-waste burning in source region of the indo-Gangetic plain. *Tellus B*, 66, ID 21026.
- Ramanathan, V., Crutzen, P. J., Lelieveld, J., Mitra, A. P., Althausen, D., Anderson, J., et al. (2001). Indian Ocean experiment: An integrated analysis of the climate forcing and effects of the great indo-Asian haze. *Journal of Geophysical Research*, 106(D22), 28,371–28,398. <https://doi.org/10.1029/2001JD900133>
- Rao, S., Klimont, Z., Leita, J., Riahi, K., van Dingenen, R., Reis, L. A., et al. (2016). A multi-model assessment of the co-benefits of climate mitigation for global air quality. *Environmental Research Letters*, 11(12), 124013. <https://doi.org/10.1088/1748-9326/11/12/124013>
- Rotach, M. W., Gohm, A., Lang, M. N., Leukauf, D., Stiperski, I., & Wagner, J. S. (2015). On the vertical exchange of heat, mass, and momentum over complex, mountainous terrain. *Frontiers in Earth Science*, 3, 76. <https://doi.org/10.3389/feart.2015.00076>

- Sahu, L. K., Sheel, V., Pandey, K., Yadav, R., Saxena, P., & Gunthe, S. (2015). Regional biomass burning trends in India: Analysis of satellite fire data. *Journal of Earth System Science*, 124(7), 1377–1387. <https://doi.org/10.1007/s12040-015-0616-3>
- Saikawa, E., Kim, H., Zhong, M., Avramov, A., Zhao, Y., Janssens-Maenhout, G., et al. (2017). Comparison of emissions inventories of anthropogenic air pollutants and greenhouse gases in China. *Atmospheric Chemistry and Physics*, 17(10), 6393–6421. <https://doi.org/10.5194/acp-17-6393-2017>
- Satheesh, S. K., Moorthy, K. K., Babu, S. S., Vinoj, V., & Dutt, C. B. S. (2008). Climate implications of large warming by elevated aerosol over India. *Geophysical Research Letters*, 35, L19809. <https://doi.org/10.1029/2008GL034944>
- Sati, A. P., & Mohan, M. (2014). Analysis of air pollution during a severe smog episode of November 2012 and the Diwali festival over Delhi, India. *International Journal of Remote Sensing*, 35(19), 6940–6954. <https://doi.org/10.1080/01431161.2014.960618>
- Seibert, P., Beyrich, F., Gryning, S.-E., Joffre, S., Rasmussen, A., & Tercier, P. (2000). Review and intercomparison of operational methods for the determination of the mixing height. *Atmospheric Environment*, 34(7), 1001–1027. [https://doi.org/10.1016/S1352-2310\(99\)00349-0](https://doi.org/10.1016/S1352-2310(99)00349-0)
- Seinfeld, J., & Pandis, S. (2006). *Atmospheric chemistry and physics: From air pollution to climate change*, (II ed.). New York: John Wiley & Sons, Inc.
- Serafin, S., Adler, B., Cuxart, J., De Wekker, S. F. J., Gohm, A., Grisogono, B., et al. (2018). Exchange processes in the atmospheric boundary layer over mountainous terrain. *Atmosphere*, 9(3), 102. <https://doi.org/10.3390/atmos9030102>
- Singh, N., Solanki, R., Ojha, N., Janssen, R. H. H., Pozzer, A., & Dhaka, S. K. (2016). Boundary layer evolution over the central Himalayas from radio wind profiler and model simulations. *Atmospheric Chemistry and Physics*, 16(16), 10,559–10,572. <https://doi.org/10.5194/acp-16-10559-2016>
- Singh, R. P., & Kaskaoutis, D. G. (2014). Crop residue burning: A threat to south Asian air quality. *Eos Transactions American Geophysical Union*, 95(37), 333–334. <https://doi.org/10.1002/2014EO370001>
- Smith, R. B., Doyle, J. D., Jiang, Q., & Smith, S. A. (2007). Alpine gravity waves: Lessons from MAP regarding mountain waves generation and braking. *Quarterly Journal of the Royal Meteorological Society*, 133(625), 917–936. <https://doi.org/10.1002/qj.103>
- Stein, A. F., Draxler, R. R., Rolph, G. D., Stunder, B. J. B., Cohen, M. D., & Ngan, F. (2015). NOAA's hysplit atmospheric transport and dispersion modeling system. *Bulletin of the American Meteorological Society*, 96(12), 2059–2077. <https://doi.org/10.1175/BAMS-D-14-00110.1>
- Stier, P., Feichter, J., Kinne, S., Kloster, S., Vignati, E., Wilson, J., Ganzeveld, L., et al. (2005). The aerosol-climate model ECHAM5-HAM. *Atmospheric Chemistry and Physics*, 5(4), 1125–1156. <https://doi.org/10.5194/acp-5-1125-2005>
- Stock, M., Cheng, Y. F., Birmili, W., Massling, A., Wehner, B., Müller, T., et al. (2011). Hygroscopic properties of atmospheric aerosol particles over the eastern Mediterranean: Implications for regional direct radiative forcing under clean and polluted conditions. *Atmospheric Chemistry and Physics*, 11(9), 4251–4271. <https://doi.org/10.5194/acp-11-4251-2011>
- Stull, R. B. (1973). Inversion rise model based on penetrative convection. *Journal of the Atmospheric Sciences*, 30(6), 1092–1099. [https://doi.org/10.1175/1520-0469\(1973\)030<1092:IRMBOP>2.0.CO;2](https://doi.org/10.1175/1520-0469(1973)030<1092:IRMBOP>2.0.CO;2)
- Stull, R. B. (1988). *An introduction to boundary layer meteorology*, *Atmospheric Sciences Library*, (p. 666). Dordrecht: Kluwer Academic Publishers. <https://doi.org/10.1007/978-94-009-3027-8>
- Tennekes, H. (1973). A model for the dynamics of the inversion above a convective boundary layer. *Journal of the Atmospheric Sciences*, 30(4), 558–567. [https://doi.org/10.1175/1520-0469\(1973\)030<0558:AMFTDO>2.0.CO;2](https://doi.org/10.1175/1520-0469(1973)030<0558:AMFTDO>2.0.CO;2)
- Twomey, S. (1977). The influence of pollution on the shortwave albedo of clouds. *Journal of the Atmospheric Sciences*, 34(7), 1149–1152. [https://doi.org/10.1175/1520-0469\(1977\)034<1149:TIOPOT>2.0.CO;2](https://doi.org/10.1175/1520-0469(1977)034<1149:TIOPOT>2.0.CO;2)
- United States Geological Survey (2016). [https://ngmdb.usgs.gov/ngmdb/ngmdb\\_home.htm](https://ngmdb.usgs.gov/ngmdb/ngmdb_home.htm). (Accessed in Jan 2017.)
- Vakkari, V., Beukes, J. P., Dal Maso, M., Aurela, M., Josipovic, M., & van Zyl, P. G. (2018). Major secondary aerosol formation in southern African open biomass burning plumes. *Nature Geoscience*, 11(8), 580–583. <https://doi.org/10.1038/s41561-018-0170-0>
- van der Werf, G. R., Randerson, J. T., Giglio, L., Collatz, G. J., Mu, M., Kasibhatla, P. S., et al. (2010). Global fire emissions and the contribution of deforestation, savanna, forest, agricultural, and peat fires (1997–2009). *Atmospheric Chemistry and Physics*, 10(23), 11,707–11,735. <https://doi.org/10.5194/acp-10-11707-2010>
- Venkataraman, C., Habib, G., Kadamba, D., Shrivastava, M., Leon, J.-F., Crouzille, B., et al. (2006). Emissions from open biomass burning in India: Integrating the inventory approach with high-resolution Moderate Resolution Imaging Spectroradiometer (MODIS) active-fire and land cover data. *Global Biogeochemical Cycles*, 20, GB2013. <https://doi.org/10.1029/2005GB002547>
- Weigel, A. P., Chow, F. K., & Rotach, M. W. (2007). The effect of mountainous topography on moisture exchange between the “surface” and the free atmosphere. *Boundary-Layer Meteorology*, 125(2), 227–244. <https://doi.org/10.1007/s10546-006-9120-2>
- Weingartner, E., Saathoff, H., Schnaiter, M., Streit, N., Bitnar, B., & Baltensperger, U. (2003). Absorption of light by soot particles: Determination of the absorption coefficient by means of aethalometers. *Journal of Aerosol Science*, 34(10), 1445–1463. [https://doi.org/10.1016/S0021-8502\(03\)00359-8](https://doi.org/10.1016/S0021-8502(03)00359-8)
- World Meteorological Organization/Global Atmosphere Watch (WMO/GAW) (2003). Aerosol measurement procedures, guidelines and recommendations, Edition 2003, GAW Report No. 153, [http://library.wmo.int/pmb\\_ged/wmo-td\\_1178.pdf](http://library.wmo.int/pmb_ged/wmo-td_1178.pdf)
- World Meteorological Organization/Global Atmosphere Watch (WMO/GAW). (2016). Aerosol measurement procedures, guidelines and recommendations, 2nd Edition 2016, GAW Report No. 227, [https://library.wmo.int/doc\\_num.php?explnum\\_id=3073](https://library.wmo.int/doc_num.php?explnum_id=3073)
- Xavier, P. K., Marzin, C., & Goswami, B. N. (2007). An objective definition of the Indian summer monsoon season and a new perspective on the ENSO–monsoon relationship. *Quarterly Journal of the Royal Meteorological Society*, 133(624), 749–764. <https://doi.org/10.1002/qj.45>
- Yokelson, R. J., Crounse, J. D., DeCarlo, P. F., Karl, T., Urbanski, S., Atlas, E., et al. (2009). Emissions from biomass burning in the Yucatan. *Atmospheric Chemistry and Physics*, 9(15), 5785–5812. <https://doi.org/10.5194/acp-9-5785-2009>
- Zardi, D., & Whiteman, C. D. (2013). Diurnal mountain wind systems. In F. Chow, S. F. J. De Wekker, & B. Synder (Eds.), *Mountain weather research and forecasting: Recent progress and current challenges*, (pp. 35–119). New York, NY: Springer.
- Zhang, K., O'Donnell, D., Kazil, J., Stier, P., Kinne, S., Lohmann, U., et al. (2012). The global aerosol-climate model ECHAM-HAM, version 2: Sensitivity to improvements in process representations. *Atmospheric Chemistry and Physics*, 12(19), 8911–8949. <https://doi.org/10.5194/acp-12-8911-2012>
- Zhang, T., Wooster, M. J., Green, D. C., & Main, B. (2015). New field-based agricultural biomass burning trace gas, PM<sub>2.5</sub>, and black carbon emission ratios and factors measured in situ at crop residue fires in Eastern China. *Atmospheric Environment*, 121, 22–34. <https://doi.org/10.1016/j.atmosenv.2015.05.010>
- Ziemba, L. D., Griffin, R. J., Cottrell, L. D., Beckman, P. J., Zhang, Q., Varner, R. K., et al. (2010). Characterization of aerosol associated with enhanced small particle number concentrations in a suburban forested environment. *Journal of Geophysical Research*, 115, D12206. <https://doi.org/10.1029/2009JD012614>
- Zou, X., Li, Y., Li, J., & Wang, B. (2016). Advection errors in an orthogonal terrain-following coordinate: Idealized 2-D experiments using steep terrains. *Atmospheric Science Letters*, 17(3), 243–250. <https://doi.org/10.1002/asl.650>